

Catastrophic overfitting is a bug but also a feature

Guillermo Ortiz-Jimenez*
EPFL

Pau de Jorge*
University of Oxford
Naver Labs Europe

Amartya Sanyal
ETH Zürich
ETH AI Center

Adel Bibi
University of Oxford

Puneet K. Dokania
University of Oxford
Five AI Ltd.

Pascal Frossard
EPFL

Grégory Rogez
Naver Labs Europe

Philip H.S. Torr
University of Oxford

Abstract

Despite clear computational advantages in building robust neural networks, adversarial training (AT) using single-step methods is unstable as it suffers from catastrophic overfitting (CO): Networks gain non-trivial robustness during the first stages of adversarial training, but suddenly reach a breaking point where they quickly lose all robustness in just a few iterations. Although some works have succeeded at preventing CO, the different mechanisms that lead to this remarkable failure mode are still poorly understood. In this work, however, we find that the interplay between the structure of the data and the dynamics of AT plays a fundamental role in CO. Specifically, through active interventions on typical datasets of natural images, we establish a causal link between the structure of the data and the onset of CO in single-step AT methods. This new perspective provides important insights into the mechanisms that lead to CO and paves the way towards a better understanding of the general dynamics of robust model construction. The code to reproduce the experiments of this paper can be found at https://github.com/gortizji/co_features.

1 Introduction

Deep neural networks are sensitive to imperceptible worst-case perturbations, also known as *adversarial perturbations* [37, 5]. As a consequence, training neural networks that are robust to such perturbations has been an active area of study in recent years [10, 27, 38, 33]. In particular, a prominent line of research, referred to as *adversarial training* (AT), focuses on online data augmentation with adversarial samples during training. However, it is well known that finding these adversarial samples for deep neural networks is an NP-hard problem [40]. In practice, this is usually overcome with various methods, referred to as *adversarial attacks* that find approximate solutions to this hard problem. The most popular attacks are based on projected gradient descent (PGD) [20] – a computationally expensive algorithm that requires multiple steps of forward and backward passes through the neural network to approximate the solution. This hinders its use in many large-scale applications motivating the use of alternative efficient *single-step* attacks [38, 10, 35].

The use of the computationally efficient single-step attacks within AT, however, comes with concerns regarding its stability. While training, although there is an initial increase in robustness, the networks often reach a breaking point beyond which they lose all gained robustness in just a few iterations [41]. This phenomenon is known as *catastrophic overfitting* (CO) [41, 2]. Nevertheless, given the clear com-

*The first two authors contributed equally. Correspondence to guillermo.ortizjimenez@epfl.ch and pau@robots.ox.ac.uk. Guillermo Ortiz-Jimenez did this work while visiting the University of Oxford.

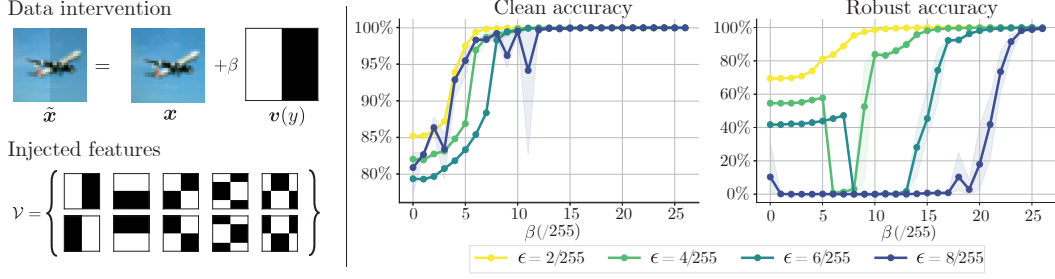


Figure 1: **Left:** Depiction of our data intervention to introduce easy-to-learn, discriminative features. **Right:** Clean and robust performance after FGSM-AT on intervened datasets $\tilde{\mathcal{D}}_\beta$. We vary the strength of the injected features β ($\beta = 0$ corresponds to the original CIFAR-10) and the robustness budget ϵ (train and test). We observe that for $\epsilon \in \{4/255, 6/255\}$ our intervention can induce CO when the injected features have strength β slightly larger than ϵ while training on the original data does not suffer CO. Results are averaged over 3 seeds and shaded areas report minimum and maximum values.

putational advantage of using single-step attacks during AT, a significant body of work has been dedicated to finding ways to circumvent CO via regularization and data augmentation [2, 6, 16, 28, 39, 9].

Despite the recent methodological advances in this front, the *root cause of CO*, experienced by single step AT methods, remains poorly understood. We show that CO is connected to properties of the data, the effectiveness of the adversarial attacks, and the training dynamics. However, due to the inherent complexity of this problem, it is difficult to disentangle these factors of variation. Hence, we argue that identifying the causal mechanisms behind this failure mode cannot be done through observations alone and requires *active interventions* [29]. That is, we need to be able to synthetically induce CO in a training context where it would not naturally happen otherwise.

In this work, we identify one such type of intervention that allows to perform abundant *in-silico* experiments to explain multiple aspects of CO. Specifically, the main contributions of our work are: (i) We show that CO can be induced by injecting easy-to-learn features that, despite being strongly discriminative, are not sufficient for robust classification by themselves (see Fig. 1). (ii) Through extensive empirical analysis, we discover that CO is connected to the preference of the network to learn different features in a dataset, an increase in non-linearity of the loss, and the existence of a learning shortcut that the network exploits to break single-step attacks. (iii) Building upon these insights, we describe and analyse a causal chain of events that can lead to CO. Overall, in this paper we show that:

Catastrophic overfitting can be a consequence of the interaction between easy- and hard-to-learn features in a dataset that can cause single-step adversarial training methods to fail.

Our findings can improve our understanding of CO as they shift focus to the study of how the data influences AT. They can help circumvent the potential pitfalls of single-step AT methods and design effective and efficient AT methods. Moreover, they also pave the way to gain further insights in the intricate dynamics of robust model construction, where the interaction between robust and non-robust features plays a key role.

2 Preliminaries and related work

Let $f_\theta : \mathbb{R}^d \rightarrow \mathcal{Y}$ denote a neural network architecture parameterized by a set of weights $\theta \in \mathbb{R}^n$ which maps input samples $x \in \mathbb{R}^d$ to $y \in \mathcal{Y} = \{1, \dots, c\}$. The objective of adversarial training (AT) is to find the network parameters $\theta \in \mathbb{R}^n$ that optimize the following min-max problem:

$$\min_{\theta} \mathbb{E}_{(x,y) \sim \mathcal{D}} \left[\max_{\|\delta\|_p \leq \epsilon} \mathcal{L}(f_\theta(x + \delta), y) \right], \quad (1)$$

where \mathcal{D} is some underlying data distribution and $\delta \in \mathbb{R}^d$ represents an adversarial perturbation. This is typically solved by alternately minimizing the outer objective and maximizing the inner one via first-order optimization procedures. The outer minimization is tackled via some standard neural network optimizer, *e.g.*, SGD, while the inner maximization problem is approximated with adversarial attacks like Fast Gradient Sign Method (FGSM) [10] and Projected Gradient Descent (PGD) [20].

Single-step AT methods are built on top of the FGSM attack. In particular, FGSM solves the linearized version of the inner maximization objective. In the ℓ_∞ case, this leads to the following attack:

$$\delta_{\text{FGSM}} = \underset{\|\delta\|_\infty \leq \epsilon}{\operatorname{argmax}} \mathcal{L}(f_\theta(\mathbf{x}), y) + \delta^\top \nabla_{\mathbf{x}} \mathcal{L}(f_\theta(\mathbf{x}), y) = \epsilon \operatorname{sign}(\nabla_{\mathbf{x}} \mathcal{L}(f_\theta(\mathbf{x}), y)). \quad (2)$$

Note that FGSM is computationally very efficient as it only requires a single forward-backward step. Unfortunately, FGSM-AT generally yields networks that stay vulnerable to multi-step attacks such as PGD [20]. In particular, Wong et al. [41] observed that FGSM-AT presents a characteristic failure mode where the robustness of the model increases during the initial training epochs, but, at a certain point in training, the model loses all its robustness within the span of a few iterations. This is known as *catastrophic overfitting* (CO). Moreover, they observed that augmenting the FGSM attack with random noise seemed to mitigate CO. However, Andriushchenko and Flammarion [2] showed that this method still leads to CO at larger ϵ . Instead, they proposed combining FGSM-AT with a smoothness regularizer $\mathcal{R}(\theta)$ (GradAlign) that encourages the cross-entropy loss to be locally linear, *i.e.*,

$$\mathcal{R}(\theta) = \mathbb{E}_{\eta, (\mathbf{x}, y)} \cos(\nabla_{\mathbf{x}} \mathcal{L}(f_\theta(\mathbf{x}), y), \nabla_{\mathbf{x}} \mathcal{L}(f_\theta(\mathbf{x} + \eta), y)) \quad \text{where} \quad \eta \sim \mathcal{U}(-\epsilon \mathbf{I}, \epsilon \mathbf{I}). \quad (3)$$

Although GradAlign succeeds in avoiding CO in all tested scenarios, optimizing it requires the computation of a second-order derivative, which adds a significant computational burden.

Other methods have been proposed that attempt to avoid CO while reducing the cost of AT [38, 35, 9, 16, 15, 19]. However these methods either only delay CO to larger ϵ radii [9, 41], are more costly [9, 35], or achieve sub-optimal robustness [9, 16]. Recently, de Jorge et al. [6] proposed N-FGSM that successfully avoids CO for large ϵ radii while incurring only a fraction of the computational cost of GradAlign. Their attack, N-FGSM, is expressed as:

$$\delta_{\text{N-FGSM}} = \eta + \epsilon \operatorname{sign}(\nabla_{\mathbf{x}} \mathcal{L}(f_\theta(\mathbf{x} + \eta), y)) \quad \text{where} \quad \eta \sim \mathcal{U}(-k \mathbf{I}, k \mathbf{I}). \quad (4)$$

and $k > 0$ is a hyperparameter that controls the strength of the noise.

On the more expensive side, multi-step attacks approximate the inner maximization with several gradient ascent steps [18, 20, 42]. Provided they use a sufficient number of steps, these methods do not suffer from CO and achieve better robustness [2, 6]. Nevertheless, using multi-step attacks in AT linearly increases the cost of training with the number of steps. Due to their superior performance and extensively validated robustness in the literature [20, 38, 42, 32], in this work, we consider multi-step methods, such as PGD, as a reference for effective AT.

Aside from proposing methods to avoid CO, some works have also studied different aspects of the training dynamics when CO occurs. While Wong et al. [41] initially suggested that CO was a result of the networks overfitting to attacks limited to the corners of the ℓ_∞ ball, this conjecture was later dismissed by Andriushchenko and Flammarion [2] who showed that AT with PGD attacks projected to the corners of the ℓ_∞ ball does not suffer from CO. On the other hand, it has been consistently reported [38, 16, 2] that networks suffering from CO exhibit a highly non-linear behaviour of their loss landscape with respect to the input compared to their CO-free counterparts. As FGSM relies on the local linearity of the loss landscape with respect to the input, this sudden increase in non-linearity of the loss renders FGSM practically ineffective [16, 15, 6]. This provides a plausible explanation for why models are not fooled by FGSM after CO. However, none of these works have managed to identify the root cause for CO that pushes the network to become strongly non-linear. In this work, we address this knowledge gap, and thoroughly explore a plausible causal mechanism that can lead single-step AT to CO.

3 Why does catastrophic overfitting happen?

Our starting point is a well known observation: while robust solutions can be attained with non-trivial changes to the standard training procedure, *e.g.*, using AT, they are not the default consequence of standard training. We argue that this is because robust classification requires leveraging additional *harder-to-learn* features than those used by default by the network in the context of standard training [12]. This intuition can be formalized in certain settings. For example, we prove in Theorem 1 that there exist learning problems where learning a robust classifier requires leveraging additional non-linear information on top of that needed for the clean solution.

Theorem 1 (Simplified). *For any $p, k \in \mathbb{N}$ such that $k < p$, there exists a family of distributions \mathcal{D}_k over \mathbb{R}^{p+1} and a concept class \mathcal{H} defined over \mathbb{R}^{p+1} such that*

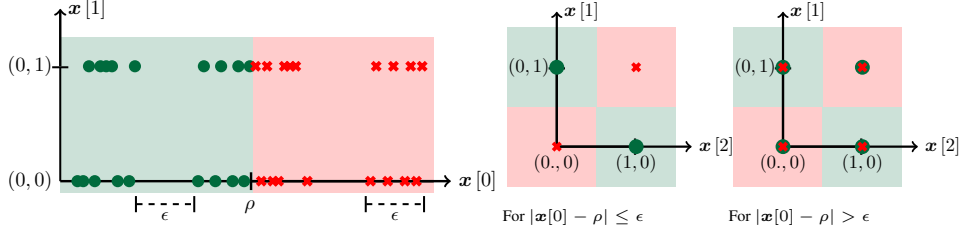


Figure 2: Illustration of the distribution in three dimensions

1. \mathcal{H} is learnable (in the PAC sense) with respect to the clean error using linear classifiers but they will be non-robust.
2. Any algorithm that robustly learns \mathcal{H} will necessarily return a non-linear classifier. In addition, the learned classifier will combine features used by the linear classifiers in the first point with other features.

Proof sketch. We provide a detailed version of Theorem 1 along with the proof in Appendix A and show a brief proof sketch here. In Fig. 2, we show an illustration of a three-dimensional data distribution (i.e., $p + 1 = 3$). The key idea of the proof is compositionality. Note that, in the left figure, the data is linearly separable with just $x[0]$ using a threshold of ρ (we argue this would be the preferred *easy-to-learn* solution when performing standard training of a network with a gradient-based optimizer). However, this threshold classifier has a small margin and is thus, not robust to adversarial perturbations. The center shows that for the points that lie close to the margin in the first coordinate ($|x[0] - \rho| \leq \epsilon$), an XOR classifier on the second and third axis can robustly separate the data. However, the right figure shows that for points that have a large margin ($|x[0] - \rho| > \epsilon$) in the first coordinate, no classifier can separate the data perfectly using just the second and third axis. This necessitates the use of the first axis for robust classification.

Theorem 1 shows that there exist distributions where robustness provably requires to learn additional non-linear information on top of the simple features which are enough for clean classification. Our empirical findings in the rest of the paper will support that this property is also satisfied by real data. That is, that real data is indeed comprised of easy-to-learn, discriminative, but non-robust features along with other harder-to-learn features that are necessary for robust classification. We will generally refer to them as *simple* or *complex* features, respectively, to reflect the intrinsic preferences of the network.

Based on this assumption, we now describe three key mechanisms, which together provide a plausible explanation for CO. In the rest of the paper, we present extensive supporting evidence for our arguments. Our first mechanism is concerned with the order at which these features are learnt during AT [14, 31] and how *robustly* separating the data may require additional information with respect to the one used in standard training [34, 21].

Mechanism 1 (Preference of the network – M1). *In the context of adversarial training in the setting described above, the network first learns the easy-to-learn features and then combines them with the other (more complex) features in an effort to increase its robustness. When the robustness requirement is lifted, the network defaults back to using just the initial non-robust features.*

Mechanism M1 conjectures that, during adversarial training, networks are biased towards first learning easy-to-learn features [14, 36] and then combining them with additional information, present in the complex features, in order to robustly separate the data. Note that this is a different phenomenon than the one observed in Shah et al. [36], who only argue that during standard training, networks learn easy features and ignore complex features altogether even when trained for a large number of epochs. Moreover, Mechanism 1 is also implying that this is a forced behaviour of the network, i.e., the network tends to forget this additional information as soon as robustness constraints are removed.

Prior work [2, 16] has observed that, when a network suffers from CO, the loss landscape becomes highly non-linear with respect to the input. In addition, some works [7, 13, 22] have also observed that the main curvature directions of the loss landscape are strongly correlated with the directions used to discriminate the data, at least on standard networks. Based on these facts, our second mechanism suggests that this increase in non-linearity is a consequence of the need for the network to fit the additional *complex* information required for robustness.

Mechanism 2 (Non-linear feature extraction – **M2**). *When combining different features to gain robustness, the network increases its non-linearity in order to learn representations that can exploit both features.*

Combining M1 and M2 provides an explanation for the increase of non-linearity AT, giving rise to a possible trigger for CO. However, it does not explain why this increase in non-linearity is worse for single-step AT than multi-step AT. Our final mechanism provides a plausible answer: It explains how the network exploits this trigger to identify a shortcut [8] which allows it to ignore the additional (complex) information needed for robustness.

Mechanism 3 (Non-linear shortcut – **M3**). *Catastrophic overfitting occurs when the increased non-linearity of the network hinders the single-step attacks from reliably approximating the inner maximization in Eq. (1). With the single-step attack rendered ineffective, the network creates a shortcut to focus only on the clean objective as long as it remains highly non-linear. This allows the network to only use the easy, non-robust features and ignore the additional robust information.*

Linking the three mechanisms mentioned above provides a plausible explanation for CO, in short:

Catastrophic overfitting is a consequence of the interaction between different features in a dataset (M1) which leads to an increase in non-linearity (M2) that causes single-step AT to fail (M3).

4 Inducing catastrophic overfitting

In Section 3, we argued that the root cause of CO stems from the bias of the network towards combining easy-to-learn features with other (more complex) features. However, directly identifying these two sets of features in a vision dataset is a difficult, if not impossible, task. Instead, as is standard practice in the field [12, 26, 3, 36, 34, 25], we rely on synthetic interventions that manipulate the data in order to make claims about its structure. In particular, we show that we can induce CO for FGSM-AT on a dataset that is synthetically intervened on and in a training regime that does not exhibit CO without the intervention *e.g.*, $\epsilon < 8/255$ during AT. Specifically, let $(\mathbf{x}, y) \sim \mathcal{D}$ be an image-label pair sample from a distribution \mathcal{D} . In order to synthetically induce the conditions in M1, we modify the *original* data \mathbf{x} by adding an *injected* feature $\mathbf{v}(y)$ that is strongly discriminative and easy-to-learn. Thus, we construct a family of *intervened datasets* $\tilde{\mathcal{D}}_\beta$ such that

$$(\tilde{\mathbf{x}}, y) \sim \tilde{\mathcal{D}}_\beta : \quad \tilde{\mathbf{x}} = \mathbf{x} + \beta \mathbf{v}(y) \quad \text{with} \quad (\mathbf{x}, y) \sim \mathcal{D}, \quad (5)$$

where $\mathbf{v}(y)$ is a label-dependent additive signal from a predefined set of linearly separable vectors $\mathcal{V} = \{\mathbf{v}(y) \mid y \in \mathcal{Y}\}$ such that $\|\mathbf{v}(y)\|_p = 1$ for all $y \in \mathcal{Y}$ and $\beta > 0$.

Properties of intervened dataset This construction has some interesting properties. Specifically, note that β controls the relative strength of the original and injected features, *i.e.*, \mathbf{x} and $\mathbf{v}(y)$, respectively. Since the injected features are linearly separable and perfectly correlated with the labels, a linear classifier can separate $\tilde{\mathcal{D}}_\beta$ for a large enough β . Moreover, as β also controls the classification margin, if $\beta \gg \epsilon$ this classifier is also robust. However, if \mathbf{x} has some components in $\text{span}(\mathcal{V})$, the interaction between \mathbf{x} and $\mathbf{v}(y)$ may decrease the robustness of a linear classifier for some β . We rigorously illustrate such a behaviour for linear classifiers in Appendix B. In short, although $\mathbf{v}(y)$ is easy-to-learn in general, the amount of additional information needed from \mathbf{x} to achieve robustness will strongly depend on β .

With the aim to control such feature interactions, we design \mathcal{V} by selecting vectors from the low-frequency components of the 2D Discrete Cosine Transform (DCT) [1] as these have a large alignment with the space of natural images that we use for our experiments (*e.g.*, CIFAR-10). Besides, and since CO has primarily been observed for ℓ_∞ perturbations, we binarize these vectors so that they only take values in ± 1 , ensuring a maximal per-pixel perturbation that satisfies $\|\mathbf{v}(y)\|_\infty = 1$. The set \mathcal{V} is illustrated in Fig. 1(left). These two design constraints also help to visually identify the alignment of adversarial perturbations δ with $\mathbf{v}(y)$ as these patterns are visually distinctive (see Fig. 3).

Injection strength (β) drives CO To test the hypotheses in Section 3, we train a PreActResNet18 [11] on different intervened versions of CIFAR-10 [17] using FGSM-AT for different robustness budgets ϵ and different β . Fig. 1 (right) shows a summary of these experiments both

in terms of clean accuracy and robustness². For clean accuracy, Fig. 1 (right) shows two distinct regimes. First, when $\beta < \epsilon$, the network achieves roughly the same accuracy by training and testing on $\tilde{\mathcal{D}}_\beta$ as by training and testing on \mathcal{D} (corresponding to $\beta = 0$). This is expected as FGSM does not suffer from CO in this setting (see Figure 1 (right)) and effectively ignores the added feature $v(y)$. Meanwhile, when $\beta > \epsilon$, the clean test accuracy is almost 100% indicating that the network heavily relies on the injected features. We provide further evidence for this in Appendix E

The behaviour with respect to robust accuracy is more diverse. For small ϵ ($\epsilon = 2/255$) the robust accuracy shows the same trend as the clean accuracy, albeit with lower values. For large ϵ ($\epsilon = 8/255$), the model incurs CO for most values of β . This is not surprising as CO has already been reported for this value of ϵ on the original CIFAR-10 dataset [41]. However, the interesting setting is for intermediate values of ϵ ($\epsilon \in \{4/255, 6/255\}$). For these settings, Fig. 1 (right) distinguishes between three distinct regimes. The first two regimes are the same as for $\epsilon = 2/255$: (i) when the strength of the injected features is weak ($\beta \ll \epsilon$), the robust accuracy is similar to that trained on the original data ($\beta = 0$) and (ii) when it is strong ($\beta \gg \epsilon$), the robust accuracy is high as the network can use only $v(y)$ to classify \tilde{x} robustly. Nevertheless, there is a third regime where the injected features are mildly robust, *i.e.*, $\beta \approx \epsilon$. Strikingly, in this regime, the training suffers from CO and the robust accuracy drops to zero. This is significant, since training on the original dataset \mathcal{D} ($\beta = 0$) does not suffer from CO for this value of ϵ ; but it does so when $\beta \approx \epsilon$. This observation aligns with the intuitions laid in the three mechanisms in Section 3 indicating that the interaction between the data and AT plays a big role in triggering CO.

We replicate these results for different \mathcal{V} 's and for ℓ_2 perturbations with similar findings in Appendix D. Results for other datasets and further details of the training protocol are given in Appendices C and D respectively. In the next section, we build upon these observations and show that the mechanisms in Section 3 indeed provide a plausible explanation for the dynamics that induce CO.

5 Analysis of induced catastrophic overfitting

Since we now have a method to intervene in the data using Eq. (5) and induce CO, we can use it to validate our explanations for CO. In particular, we explore how the structure of the dataset features can lead to CO for FGSM-AT. First, we show that, indeed, the network combines information from both the easy-to-learn and the more complex features in order to improve robustness as described in M1. Then, we study the non-linearity of the network during AT and show how it leads to CO following M3; this chain of events is driven by the interaction between the features as per M2.

5.1 Robust solutions combine easy- and hard-to-learn features

We now show that, in the regime where $\beta \approx \epsilon$, to achieve a high robust accuracy on the intervened dataset $\tilde{\mathcal{D}}_\beta$, the network uses information from both the original dataset \mathcal{D} and the injected features in \mathcal{V} . However, when trained without any adversarial constraints *i.e.*, for standard training, the network only uses the features in \mathcal{V} and achieves close to perfect clean accuracy.

Testing the preference for different features In order to demonstrate this empirically, we perform standard, FGSM-AT, and PGD-AT training of a PreActResNet18 on the intervened dataset $\tilde{\mathcal{D}}_\beta$ (as described in Section 4) with $\beta = 8/255$ and $\epsilon = 6/255$. First, note that Fig. 1 (right) shows that an FGSM-AT model suffers from CO when trained on this intervened dataset. Next, we construct three different tests sets and evaluate the clean and robust accuracy of the networks on them in Fig. 4. The



Figure 3: Different samples of the intervened dataset $\tilde{\mathcal{D}}_\beta$, and FGSM perturbations before and after CO. While prior to CO perturbations focus on the injected features, after CO they become noisy.

²Throughout the paper, robustness is measured against strong PGD attacks with 50 iterations and 10 restarts.

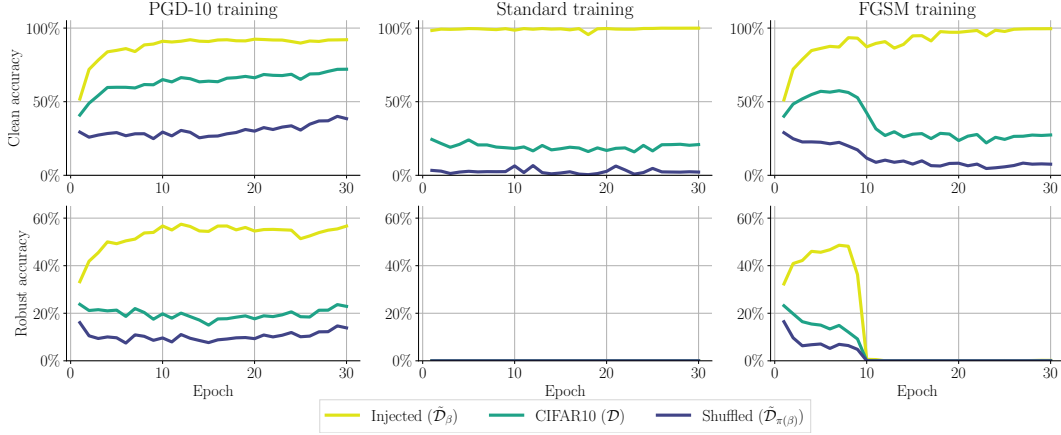


Figure 4: Clean (**top**) and robust (**bottom**) accuracy on 3 different test sets: (i) the original CIFAR-10 (\mathcal{D}), (ii) the dataset with injected features $\tilde{\mathcal{D}}_\beta$ and (iii) the dataset with shuffled injected features $\tilde{\mathcal{D}}_{\pi(\beta)}$. All training runs use $\beta = 8/255$ and $\epsilon = 6/255$ (where FGSM-AT suffers CO).

three different test sets are: (i) CIFAR-10 test set with injected features ($\tilde{\mathcal{D}}_\beta$), (ii) original CIFAR-10 test set (\mathcal{D}), and (iii) CIFAR-10 test set with shuffled injected features ($\tilde{\mathcal{D}}_{\pi(\beta)}$) where the additive signals are correlated with a permuted set of labels, *i.e.*,

$$(\tilde{\mathbf{x}}^{(\pi)}, y) \sim \tilde{\mathcal{D}}_{\pi(\beta)} : \quad \tilde{\mathbf{x}}^{(\pi)} = \mathbf{x} + \beta \mathbf{v}(\pi(y)) \quad \text{with} \quad (\mathbf{x}, y) \sim \mathcal{D} \quad \text{and} \quad \mathbf{v} \in \mathcal{V}. \quad (6)$$

Here, $\pi : \mathcal{Y} \rightarrow \mathcal{Y}$ is a fixed permutation operator that shuffles the labels. Note that evaluating these networks (trained on $\tilde{\mathcal{D}}_\beta$) on data from $\tilde{\mathcal{D}}_{\pi(\beta)}$ exposes them to contradictory information, since \mathbf{x} and $\mathbf{v}(\pi(y))$ are correlated with different labels in $\tilde{\mathcal{D}}_\beta$. Thus, depending on which feature the networks rely more on for classification, their performance will vary among these three datasets as discussed below.

Standard training and PGD Figure 4(left) shows that the PGD-trained network achieves a robust solution using both \mathcal{D} and \mathcal{V} . This is clear as the PGD-trained network achieves better than trivial accuracy on both \mathcal{D} , where there is no information coming from \mathcal{V} , as well as $\tilde{\mathcal{D}}_{\pi(\beta)}$ where, by construction (see Eq. (6)), the features from \mathcal{V} are correlated with an incorrect label. Besides, the fact that the network achieves higher accuracy on samples from $\tilde{\mathcal{D}}_\beta$ than on those of \mathcal{D} implies that it also leverages \mathcal{V} for classification. This provides evidence for mechanism M1. On the other hand, standard training shows a completely different behaviour (see Fig. 4 (center)). In this case, even though the network achieves excellent clean accuracy on $\tilde{\mathcal{D}}_\beta$, its accuracy on \mathcal{D} is nearly trivial. Moreover, when asked to classify $\tilde{\mathcal{D}}_{\pi(\beta)}$, its accuracy is almost zero. This clearly indicates that the network, obtained from standard training, ignores the information present in \mathcal{D} and only uses the non-robust features from \mathcal{V} for classification. As a result, the classifier, in this case, is non-robust. These two observations align with the idea that the network has a preference for easy-to-learn solutions *e.g.*, features in \mathcal{V} (as shown by standard training) which, when not sufficient to classify robustly, are combined with more complex features *e.g.*, in \mathcal{D} (as shown by PGD-AT).

FGSM training The behaviour of the FGSM training in Fig. 4(right) highlights this preference even further. First, note that FGSM-AT undergoes CO around epoch 10 when the robust accuracy on $\tilde{\mathcal{D}}_\beta$ suddenly drops to zero despite a high clean accuracy on $\tilde{\mathcal{D}}_\beta$. Next, as seen in Fig. 4 (top right), FGSM-AT presents two distinct phases during training: (i) Prior to CO, when the robust accuracy on $\tilde{\mathcal{D}}_\beta$ is non-zero, the network leverages features from both \mathcal{D} and \mathcal{V} , as observed for PGD. (ii) However, with the onset of CO, both the clean and robust accuracy on \mathcal{D} and $\tilde{\mathcal{D}}_{\pi(\beta)}$ drops, exhibiting behavior similar to standard training. This indicates that, post-CO, the network forgets the information from \mathcal{D} and solely relies on features in \mathcal{V} . To understand this behavior, recall mechanism M3. It suggests that when CO occurs, FGSM attacks are rendered ineffective thus effectively eliminating the robustness constraints. At that moment, as shown in Fig. 4(right), around epoch 10, the network defaults back to using only the easy-to-learn features ($\mathbf{v}(y) \in \mathcal{V}$) and performance on the original \mathcal{D} drops.

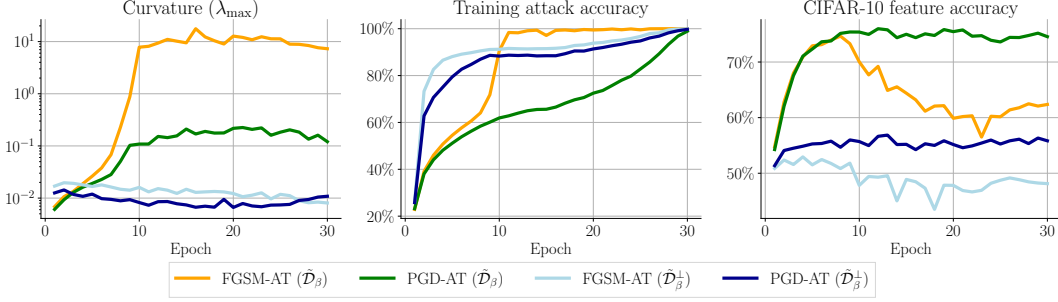


Figure 5: Evolution of different metrics for FGSM-AT and PGD-AT on 2 datasets: (i) with injected features ($\tilde{\mathcal{D}}_\beta$) and (ii) with orthogonally projected features, i.e. with no interaction between the original and injected features ($\tilde{\mathcal{D}}_\beta^\perp$). AT is performed for $\beta = 8/255$ and $\epsilon = 6/255$ (where FGSM suffers CO).

5.2 Curvature explosion drives catastrophic overfitting

We further investigate the mechanisms formulated in Section 3, and move on to the study of the non-linearity of the loss. In particular, we track the local curvature of the loss landscape during training as a strong proxy for non-linearity and show that, in line with mechanism M3, the non-linearity explodes during CO. Inspired by Moosavi-Dezfooli et al. [23], we use the average maximum eigenvalue of the Hessian on $N = 100$ fixed training points $\bar{\lambda}_{\max} = \frac{1}{N} \sum_{n=1}^N \lambda_{\max}(\nabla_{\tilde{\mathbf{x}}}^2 \mathcal{L}(f_{\theta}(\tilde{\mathbf{x}}_n), y_n))$ to estimate curvature and record it throughout training. Fig. 5(left) shows the result of this experiment for FGSM-AT (orange line) and PGD-AT (green line) training on $\tilde{\mathcal{D}}_\beta$ with $\beta = 8/255$ and $\epsilon = 6/255$. Recall that this training regime exhibits CO with FGSM-AT around epoch 10 (see Fig. 4(left)).³

Curvature increase Interestingly, we observe that even before the onset of CO, both FGSM-AT and PGD-AT show a steep increase in curvature (the y -axis is in logarithmic scale). While right before the 10th epoch, there is a large increase in the curvature for PGD-AT, it stabilizes soon after and for the rest of training. Prior work has observed that PGD-AT acts as a regularizer on the curvature [23, 30] which explains why we observe that this curvature increase is eventually dampened in the PGD-AT run. Unlike PGD-AT, FGSM-AT is based on a linear (first order) approximation of the loss, which means that it is not effective at regularising the curvature, which is a second-order property of the loss surface. Indeed, we see that FGSM-AT cannot contain the curvature increase, which eventually explodes around the 10th epoch and saturates at the moment that the training attack accuracy reaches its maximum. Quite remarkably, the final curvature of the FGSM-AT model is 100 times that of the PGD-AT model.

Meaningless perturbations The fact that the curvature increases rapidly during CO, when the attack accuracy also increases, agrees with the findings of Andriushchenko and Flammarion [2], who claimed that CO happens as a result of gradient misalignment, *i.e.*, the loss becomes highly non-linear and thus reduces the success rate of FGSM. To show that CO indeed occurs due to the increased curvature breaking FGSM, we visualise the adversarial perturbations before and after CO. As observed in Fig. 3, before CO, the adversarial perturbations point in the direction of \mathcal{V} , albeit with some corruptions originating from \mathbf{x} . Nonetheless, after CO, the new adversarial perturbations point towards meaningless directions; they do not align with \mathcal{V} even though the network is heavily reliant on this information for classifying the data (cf. Section 5.1). This reinforces the idea that the increase in curvature indeed causes a breaking point after which FGSM is no longer an effective adversarial attack. We would like to highlight that this behaviour of the adversarial perturbations after CO is radically different from the behaviour on standard and robust networks (in the absence of CO) where adversarial perturbations and curvature are strongly aligned with discriminative directions [12, 13, 7].

5.3 Curvature increase is a result of interaction between features

Why does the network increase the curvature in the first place? In Section 5.1, we observed that this is a shared behaviour of PGD-AT and FGSM-AT, at least during the stage before CO. Therefore, it should not be a mere “bug”. As presented in mechanisms M1 and M2, we conjecture that the

³Results for other parameters and for the original \mathcal{D} are provided in Appendix F.

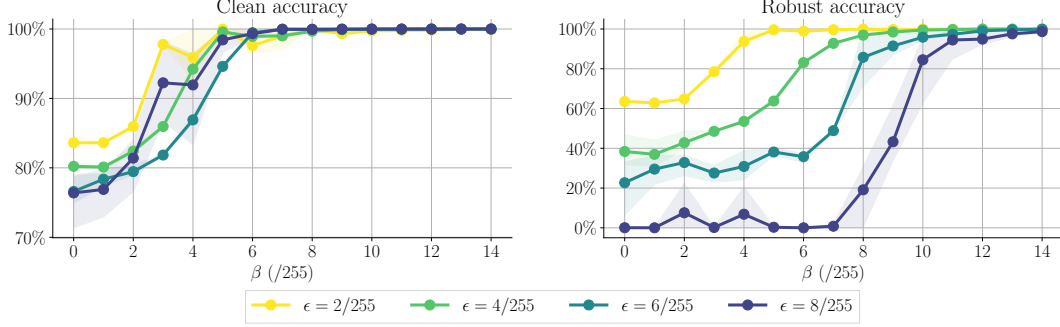


Figure 6: Clean (**left**) and robust (**right**) accuracy after FGSM-AT on a dataset with orthogonally injected features $\tilde{\mathcal{D}}_\beta^\perp$ i.e. no interaction between original and injected features. We train while varying the strength of the injected features and the robustness budget ϵ .

curvature increases as a result of the interaction between features of the dataset which forces the network to increase its non-linearity in order to combine them effectively to obtain a robust model.

Curvature does not increase without interaction To demonstrate this, we perform a new experiment in which we again intervene on the dataset \mathcal{D} (as in Section 4). However, this time, we ensure that there is no interaction, *i.e.*, correlation, between the injected features $\mathbf{v}(y)$ and the features from \mathcal{D} . We do so by creating $\tilde{\mathcal{D}}_\beta^\perp$ such that:

$$(\tilde{\mathbf{x}}^\perp, y) \sim \tilde{\mathcal{D}}_\beta^\perp : \quad \tilde{\mathbf{x}}^\perp = \mathcal{P}_{\mathcal{V}^\perp}(\mathbf{x}) + \beta \mathbf{v}(y) \quad \text{with} \quad (\mathbf{x}, y) \sim \mathcal{D} \quad \text{and} \quad \mathbf{v}(y) \in \mathcal{V} \quad (7)$$

where $\mathcal{P}_{\mathcal{V}^\perp}$ denotes the projection operator onto the orthogonal complement of \mathcal{V} . Since the injected features $\mathbf{v}(y)$ are orthogonal to \mathcal{D} , a simple linear classifier relying only on $\mathbf{v}(y)$ can robustly separate the data up to a radius that depends solely on β (see the theoretical construction in Appendix B).

Interestingly, we find that, in this dataset, none of the (β, ϵ) configurations used in Fig. 6 induce CO. Here, we observe only two regimes: one that ignores \mathcal{V} (when $\beta < \epsilon$) and the one that ignores \mathcal{D} (when $\beta > \epsilon$). This supports our conjecture that the interaction between the features of \mathbf{x} and $\mathbf{v}(y)$ is the true cause of CO in $\tilde{\mathcal{D}}_\beta$. Moreover, Fig. 5 (left) shows that, when performing either FGSM-AT (light blue) or PGD-AT (dark blue) on $\tilde{\mathcal{D}}_\beta^\perp$, the curvature is consistently low. This agrees with the fact that in this case there is no need for the network to combine the injected and the original features to achieve robustness and hence the network does not need to increase its non-linearity to separate the data.

Non-linear feature extraction Finally, we perform an experiment to gauge the connection between the quality of feature representations and the network’s curvature: We train multiple logistic regression models to classify \mathcal{D} using the feature representations (output of the penultimate layer) of networks trained on $\tilde{\mathcal{D}}_\beta$. Note that the accuracy of these simple classifiers strictly depends on how well the network (trained on $\tilde{\mathcal{D}}_\beta$) has learned to combine information from both \mathcal{D} and \mathcal{V} , as explained in M2. We will call this metric *feature accuracy*. Figure 5(right) shows the evolution of the feature accuracy of the networks during training. Observe that, for PGD-AT (green), the feature accuracy on \mathcal{D} progressively grows during training. The high values of feature accuracy indicate that this network has learned to meaningfully extract information from \mathcal{D} , even if it was trained on $\tilde{\mathcal{D}}_\beta$. Moreover, note that the feature accuracy closely matches the curvature trajectory in Fig. 5 (left). On the other hand, for FGSM-AT the feature accuracy has two phases: First, it grows at the same rate as for the PGD-AT network, but when CO happens, it starts to decrease. Nonetheless, when CO happens, the curvature does not decrease. We argue that this happens because the network has learned a shortcut in order to ignore \mathcal{D} . As described in mechanism M3, if the curvature is very high, FGSM is rendered ineffective and allows the network to focus only on the easy-to-learn, non-robust, features. On the other hand, if we use the features from networks trained on $\tilde{\mathcal{D}}_\beta^\perp$ we observe that the accuracy on \mathcal{D} is always low. This reinforces the view that the network is increasing the curvature in order to improve its feature representation: In $\tilde{\mathcal{D}}_\beta^\perp$ the network does not need to combine information from both \mathcal{D} and \mathcal{V} to become robust, and hence it does not learn to disentangle \mathcal{D} using mechanism M2.

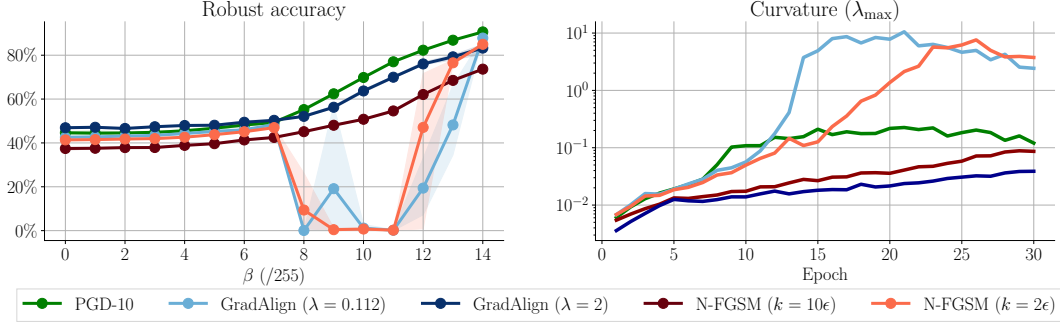


Figure 7: **Left:** Clean and robust performance after AT with GradAlign, N-FGSM and PGD-10 on $\tilde{\mathcal{D}}_\beta$ at $\epsilon = 6/255$. Results averaged over three random seeds and shaded areas report minimum and maximum values. **Right:** Curvature evolution when training on $\tilde{\mathcal{D}}_\beta$ at $\epsilon = 6/255$ and $\beta = 8/255$.

6 Further insights and discussion

Our proposed dataset intervention, defined in Section 4, allowed us to gain a better understanding of the chain of events that lead to CO. In this section, we focus our attention on methods that can prevent CO and analyze them in the context of our framework to provide further insights.

GradAlign and N-FGSM prevent CO on $\tilde{\mathcal{D}}_\beta$ In Fig. 7, we show the robust accuracy (left) and curvature (right) of models trained with GradAlign [2] and N-FGSM [6] on the intervened dataset $\tilde{\mathcal{D}}_\beta$ for varying β . Figure 7 (left) shows that both methods are able to prevent CO on our intervened dataset for suitable choices of the regularisation parameter *i.e.*, λ for GradAlign and k for N-FGSM. This suggests that the mechanism by which our intervention induces CO is similar to how it occurs in real datasets. However, for certain values of β , both GradAlign and N-FGSM require stronger regularization. Thus, the regularization strength is not only a function of ϵ , as discussed in their respective manuscripts [2, 6], but also of the signal strength β . As β increases, $v(y)$ becomes more discriminative creating a stronger incentive for the network to use it. Using the mechanisms M1, M2, and M3, as discussed in Section 5, we argue that this increases the chances for CO. Moreover, Fig. 7 shows that the curvature of N-FGSM and GradAlign AT stabilizes with a trend similar to PGD-AT and stronger regularizations dampens the increase of the curvature even further. This agrees with mechanism M3 as it shows that preventing the curvature from exploding can indeed prevent CO.

Can data interventions avoid CO? Section 4 shows that it is possible to induce CO through data manipulations. But is the opposite also true that CO can be avoided using data manipulations? We find that this is indeed possible on CIFAR-10. Table 1 shows that removing the high frequency components of \mathcal{D} consistently prevents CO at $\epsilon = 8/255$ (where FGSM-AT fails). However, applying the same low-pass technique and training with $\epsilon = 16/255$ does not prevent CO. We conjecture that this is because features which are robust at $\epsilon = 8/255$ in the low pass version of CIFAR-10 might not be robust at $\epsilon = 16/255$, therefore forcing the network to combine more complex features. More generally, we point out that this method is difficult to generalise, as it requires identifying the different features that interact to cause CO in common vision datasets, which is an extremely difficult problem.

Table 1: Clean and robust accuracies of FGSM-AT and PGD-AT trained networks on CIFAR-10 and the low pass version described in Ortiz-Jimenez et al. [26] at different ϵ .

Method (ϵ)	Original		Low pass	
	Clean	Robust	Clean	Robust
FGSM ($8/255$)	85.6	0.0	81.1	47.0
PGD ($8/255$)	80.9	50.6	80.3	49.7
FGSM ($16/255$)	76.3	0.0	78.6	0.0
PGD ($16/255$)	68.0	29.2	66.9	28.4

7 Concluding remarks

In this work, we have presented a thorough empirical study to establish a causal link between the features of the data and the onset of CO in FGSM-AT. Specifically, using controlled data interventions we have seen that, (i) when imposed with robustness constraints, networks have a preference to combine easy-to-learn, discriminative, but non-robust features with other (complex) features to achieve

robustness. (ii) Moreover, if there is an interaction between these features the network tends to increase its non-linearity. (iii) If unchecked, this increase in non-linearity can trigger CO. This new perspective has allowed us to shed new light on the mechanisms that trigger CO, as it shifted our focus towards studying the way the data structure influences the learning algorithm. We believe this opens the door to promising future work focused on understanding the intricacies of these learning mechanisms. In general, we consider that deriving methods that allow to inspect the data and identify how different features of a dataset interact within each other is another interesting avenue for future work.

Acknowledgements

We thank Maksym Andriushchenko, Apostolos Modas, Seyed-Mohsen Moosavi-Dezfooli and Ricardo Volpi for the fruitful discussions and feedback. This work is supported by the UKRI grant: Turing AI Fellowship EP/W002981/1 and EPSRC/MURI grant: EP/N019474/1. We would also like to thank the Royal Academy of Engineering and FiveAI. Guillermo Ortiz-Jimenez acknowledges travel support from ELISE (GA no 951847) in the context of the ELLIS PhD Program. Amartya Sanyal acknowledges partial support from the ETH AI Center.

References

- [1] N. Ahmed, T. Natarajan, and K. R. Rao. Discrete Cosine Transform. *IEEE Transactions on Computers*, 1974.
- [2] Maksym Andriushchenko and Nicolas Flammarion. Understanding and improving fast adversarial training. In *Neural Information Processing Systems (NeurIPS)*, 2020.
- [3] Devansh Arpit, Stanisław Jastrzebski, Nicolas Ballas, David Krueger, Emmanuel Bengio, Maxinder S Kanwal, Tegan Maharaj, Asja Fischer, Aaron Courville, Yoshua Bengio, and Simon Lacoste-Julien. A closer look at memorization in deep networks. In *International Conference on Machine Learning (ICML)*, 2017.
- [4] James Aspnes, Richard Beigel, Merrick Furst, and Steven Rudich. The expressive power of voting polynomials. *Combinatorica*, 1994.
- [5] Adith Bloor, Xin He, Christopher D. Gill, Yevgeniy Vorobeychik, and Xuan Zhang. Simple physical adversarial examples against end-to-end autonomous driving models. *arxiv:1903.05157*, 2019.
- [6] Pau de Jorge, Adel Bibi, Riccardo Volpi, Amartya Sanyal, Philip H. S. Torr, Grégory Rogez, and Puneet K. Dokania. Make some noise: Reliable and efficient single-step adversarial training. *arxiv:2202.01181*, 2022.
- [7] Alhussein Fawzi, Seyed-Mohsen Moosavi-Dezfooli, Pascal Frossard, and Stefano Soatto. Empirical study of the topology and geometry of deep networks. In *IEEE Conference on Computer Vision and Pattern Recognition (CVPR)*, 2018.
- [8] R. Geirhos, J.-H. Jacobsen, C. Michaelis, R. Zemel, W. Brendel, M. Bethge, and F. A. Wichmann. Shortcut learning in deep neural networks. *Nature Machine Intelligence*, 2020.
- [9] Zeinab Golgooni, Mehrdad Saberi, Masih Eskandar, and Mohammad Hossein Rohban. Zerograd: Mitigating and explaining catastrophic overfitting in fgsm adversarial training. *arXiv:2103.15476*, 2021.
- [10] Ian Goodfellow, Jonathon Shlens, and Christian Szegedy. Explaining and harnessing adversarial examples. *International Conference on Learning Representations (ICLR)*, 2015.
- [11] Kaiming He, Xiangyu Zhang, Shaoqing Ren, and Jian Sun. Identity mappings in deep residual networks. In *European Conference on Computer Vision (ECCV)*, 2016.
- [12] Andrew Ilyas, Shibani Santurkar, Dimitris Tsipras, Logan Engstrom, Brandon Tran, and Aleksander Madry. Adversarial examples are not bugs, they are features. *Neural Information Processing Systems (NeurIPS)*, 2019.
- [13] Saumya Jetley, Nicholas Lord, and Philip Torr. With friends like these, who needs adversaries? *Neural Information Processing Systems (NeurIPS)*, 2018.

- [14] Dimitris Kalimeris, Gal Kaplun, Preetum Nakkiran, Benjamin Edelman, Tristan Yang, Boaz Barak, and Haofeng Zhang. Sgd on neural networks learns functions of increasing complexity. *Advances in neural information processing systems*, 32, 2019.
- [15] Peilin Kang and Seyed-Mohsen Moosavi-Dezfooli. Understanding catastrophic overfitting in adversarial training. *arXiv:2105.02942*, 2021.
- [16] Hoki Kim, Woojin Lee, and Jaewook Lee. Understanding catastrophic overfitting in single-step adversarial training. In *AAAI Conference on Artificial Intelligence (AAAI)*, 2021.
- [17] Alex Krizhevsky and Geoffrey Hinton. Learning multiple layers of features from tiny images. *Master’s thesis, Department of Computer Science, University of Toronto*, 2009.
- [18] Alexey Kurakin, Ian Goodfellow, and Samy Bengio. Adversarial machine learning at scale. In *International Conference on Learning Representations (ICLR)*, 2017.
- [19] Bai Li, Shiqi Wang, Suman Jana, and Lawrence Carin. Towards understanding fast adversarial training. *arXiv:2006.03089*, 2020.
- [20] Aleksander Madry, Aleksandar Makelov, Ludwig Schmidt, Dimitris Tsipras, and Adrian Vladu. Towards deep learning models resistant to adversarial attacks. In *International Conference on Learning Representations (ICLR)*, 2018.
- [21] Omar Montasser, Steve Hanneke, and Nathan Srebro. Vc classes are adversarially robustly learnable, but only improperly. In *Annual Conference on Learning Theory (COLT)*, 2019.
- [22] Seyed-Mohsen Moosavi-Dezfooli, Alhussein Fawzi, Omar Fawzi, Pascal Frossard, and Stefano Soatto. Robustness of classifiers to universal perturbations: A geometric perspective. In *International Conference on Learning Representations (ICLR)*, 2018.
- [23] Seyed-Mohsen Moosavi-Dezfooli, Alhussein Fawzi, Jonathan Uesato, and Pascal Frossard. Robustness via curvature regularization, and vice versa. In *IEEE Conference on Computer Vision and Pattern Recognition (CVPR)*, 2019.
- [24] Yuval Netzer, Tao Wang, Adam Coates, Alessandro Bissacco, Bo Wu, and Andrew Y Ng. Reading digits in natural images with unsupervised feature learning. In *Neural Information Processing Systems (NeurIPS), Workshops*, 2011.
- [25] Guillermo Ortiz-Jimenez, Apostolos Modas, Seyed-Mohsen Moosavi, and Pascal Frossard. Neural anisotropy directions. *Neural Information Processing Systems (NeurIPS)*, 2020.
- [26] Guillermo Ortiz-Jimenez, Apostolos Modas, Seyed-Mohsen Moosavi, and Pascal Frossard. Hold me tight! influence of discriminative features on deep network boundaries. *Neural Information Processing Systems (NeurIPS)*, 2020.
- [27] Nicolas Papernot, Patrick McDaniel, Xi Wu, Somesh Jha, and Ananthram Swami. Distillation as a defense to adversarial perturbations against deep neural networks. In *IEEE symposium on security and privacy (SP)*, 2016.
- [28] Geon Yeong Park and Sang Wan Lee. Reliably fast adversarial training via latent adversarial perturbation. In *International Conference on Learning Representations (ICLR), Workshops*, 2021.
- [29] Judea Pearl and Dana Mackenzie. *The Book of Why: The New Science of Cause and Effect*. Basic Books, 2018.
- [30] Chongli Qin, James Martens, Sven Gowal, Dilip Krishnan, Krishnamurthy Dvijotham, Alhussein Fawzi, Soham De, Robert Stanforth, and Pushmeet Kohli. Adversarial robustness through local linearization. In *Neural Information Processing Systems (NeurIPS)*, 2019.
- [31] Nasim Rahaman, Aristide Baratin, Devansh Arpit, Felix Draxler, Min Lin, Fred Hamprecht, Yoshua Bengio, and Aaron Courville. On the spectral bias of neural networks. In *International Conference on Machine Learning (ICML)*, 2019.
- [32] Leslie Rice, Eric Wong, and Zico Kolter. Overfitting in adversarially robust deep learning. In *International Conference on Machine Learning (ICML)*, 2020.
- [33] Amartya Sanyal, Varun Kanade, Philip HS Torr, and Puneet K Dokania. Robustness via deep low-rank representations. *arXiv:1804.07090*, 2018.
- [34] Amartya Sanyal, Puneet K. Dokania, Varun Kanade, and Philip Torr. How benign is benign overfitting ? In *International Conference on Learning Representations (ICLR)*, 2021.

- [35] Ali Shafahi, Mahyar Najibi, Mohammad Amin Ghiasi, Zheng Xu, John Dickerson, Christoph Studer, Larry S Davis, Gavin Taylor, and Tom Goldstein. Adversarial training for free! *Neural Information Processing Systems (NeurIPS)*, 2019.
- [36] Harshay Shah, Kaustav Tamuly, Aditi Raghunathan, Prateek Jain, and Praneeth Netrapalli. The pitfalls of simplicity bias in neural networks. *Neural Information Processing Systems (NeurIPS)*, 2020.
- [37] Christian Szegedy, Wojciech Zaremba, Ilya Sutskever, Joan Bruna, Dumitru Erhan, Ian Goodfellow, and Rob Fergus. Intriguing properties of neural networks. In *International Conference on Learning Representations (ICLR)*, 2014.
- [38] Florian Tramèr, Alexey Kurakin, Nicolas Papernot, Ian Goodfellow, Dan Boneh, and Patrick McDaniel. Ensemble adversarial training: Attacks and defenses. In *International Conference on Learning Representations (ICLR)*, 2018.
- [39] BS Vivek and R Venkatesh Babu. Single-step adversarial training with dropout scheduling. In *IEEE Conference on Computer Vision and Pattern Recognition (CVPR)*, 2020.
- [40] Lily Weng, Huan Zhang, Hongge Chen, Zhao Song, Cho-Jui Hsieh, Luca Daniel, Duane Boning, and Inderjit Dhillon. Towards fast computation of certified robustness for relu networks. In *International Conference on Machine Learning (ICML)*, 2018.
- [41] Eric Wong, Leslie Rice, and J. Zico Kolter. Fast is better than free: Revisiting adversarial training. In *International Conference on Learning Representations (ICLR)*, 2020.
- [42] Hongyang Zhang, Yaodong Yu, Jiantao Jiao, Eric Xing, Laurent El Ghaoui, and Michael Jordan. Theoretically principled trade-off between robustness and accuracy. In *International Conference on Machine Learning (ICML)*, 2019.

A Robust classification can require non-linear features

We now provide a rigorous theoretical example of a learning problem that provably requires additional complex information for robust classification, even though it can achieve good clean performance using only simple features. In particular we prove a rigorous version of Theorem 1 below.

Given some $p \in \mathbb{N}$, let \mathbb{R}^{p+1} be the input domain. A concept class, defined over \mathbb{R}^{p+1} is a set of functions from \mathbb{R}^{p+1} to $\{0, 1\}$. A hypothesis h is s -non-linear if the polynomial with the smallest degree that can represent h has a degree (largest order polynomial term) of s .

Using these concepts we now state the main result.

Theorem 2. *For any $p, k \in \mathbb{N}, \epsilon < 0.5$ such that $k < p$, there exists a family of distributions \mathcal{D}_k over \mathbb{R}^{p+1} and a concept class \mathcal{H} defined over \mathbb{R}^{p+1} such that*

1. \mathcal{H} is PAC learnable (with respect to the clean error) with a linear (degree 1) classifier. However, \mathcal{H} is not robustly learnable with any linear classifier.
2. There exists an efficient learning algorithm, that given a dataset sampled i.i.d. from a distribution $\mathcal{D} \in \mathcal{D}_k$ robustly learns \mathcal{H} .

In particular, the algorithm returns a k -non-linear classifier and in addition, the returned classifier also exploits the linear features used by the linear non-robust classifier.

Proof. We now define the construction of the distributions in \mathcal{D}_k . Every distribution \mathcal{D} in the family of distribution \mathcal{D}_k is uniquely defined by three parameters: a threshold parameter $\rho \in \{4t\epsilon : t \in \{0, \dots, k\}\}$ (one can think of this as the non-robust, easy-to-learn feature), a p dimensional bit vector $c \in \{0, 1\}^p$ such that $\|c\|_1 = k$ (this is the non-linear but robust feature) and ϵ . Therefore, given ρ and c (and ϵ which we discuss when necessary and ignore from the notation for simplicity), we can define the distribution $\mathcal{D}^{c,\rho}$. We provide an illustration of this distribution for $p = 2$ in Figure 8.

Sampling the robust non-linear feature To sample a point $(x, y) \in \mathbb{R}^{p+1}$ from the distribution $\mathcal{D}^{c,\rho}$, first, sample a random bit vector $\hat{x} \in \mathbb{R}^p$ from the uniform distribution over the boolean hypercube $\{0, 1\}^p$. Let $\hat{y} = \sum_{i=1}^{p-1} \hat{x}[i] \cdot c[i] \pmod{2}$ be the label of the parity function with respect to c evaluated on \hat{x} . The marginal distribution over \hat{y} , if sampled this way, is equivalent to the Bernoulli distribution with parameter $\frac{1}{2}$. To see why, fix all bits in the input except one (chosen arbitrarily from the variables of the parity function), which is distributed uniformly over $\{0, 1\}$. It is easy to see that this forces the output of the parity function to be distributed uniformly over $\{0, 1\}$ as well. Repeating this process for all dichotomies of $p - 1$ variables of the parity function proves the desired result. Intuitively, \hat{x} constitutes the robust non-linear feature of this distribution.

Sampling the non-robust linear feature To ensure that \hat{x} is not perfectly correlated with the true label, we sample the true label y from a Bernoulli distribution with parameter $\frac{1}{2}$. Then we sample the non-robust feature x_1 as follows

$$x_1 \sim \begin{cases} \text{Unif}(X_1^-) & y = 0 \wedge \hat{y} = 0 \\ \text{Unif}(X_1^+) & y = 1 \wedge \hat{y} = 1 \\ \text{Unif}(X_2^-) & y = 0 \wedge \hat{y} = 1 \\ \text{Unif}(X_2^+) & y = 1 \wedge \hat{y} = 0 \end{cases}$$

where

$$X_1^+ = [\rho, \rho + \epsilon] \text{ and } X_2^+ = [(\rho + 2\epsilon, \rho + 3\epsilon)], X_1^- = [\rho - \epsilon, \rho] \text{ and } X_2^- = [(\rho - 3\epsilon, \rho - 2\epsilon)].$$

Finally, we return (x, y) where $x = (x_1; \hat{x})$ is the concatenation of x_1 and \hat{x} .

Linear non-robust solution First, we show that there is a linear, accurate, but non-robust solution to this problem. To obtain this solution, sample an m -sized dataset $S_m = \{(x_1, y_1), \dots, (x_m, y_m)\} \in \mathbb{R}^{p+1} \times \{-1, 1\}$ from the distribution $\mathcal{D}^{c,\rho}$. Ignore all, except the first coordinate, of the covariates of the dataset to create $S_m^0 = \{(x_1[0], y_1) \dots (x_m[0], y_m)\}$ where $S_i[j]$ indexes the j^{th} coordinate of the i^{th} element of the dataset. Then, sort S_m^0 on the basis of the covariates (i.e., the first coordinate). Let $\hat{\rho}$ be the largest element whose label is 0.

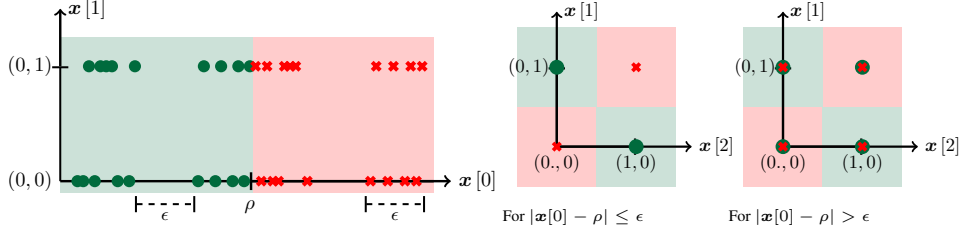


Figure 8: Illustration of one possible distribution $\mathcal{D}^{c,\rho}$ in three dimensions. The data is linearly separable in the direction $x[0]$ but has a very small margin in that direction. Leveraging $x[1]$ and $x[2]$ additionally, we see how the data can indeed be separated robustly, albeit non-linearly.

Define $f_{\text{lin},\hat{\rho}}$ as the linear threshold function on the first coordinate i.e. $f_{\text{lin},\hat{\rho}}(\mathbf{x}) = \mathbb{I}\{x[0] \geq \hat{\rho}\}$. By construction, $f_{\text{lin},\hat{\rho}}$ accurately classifies all points in S_m . The VC dimension of a linear threshold function in 1 dimension is 2. Then, using standard VC sample complexity upper bounds⁴ for consistent learners, if $m \geq \kappa_0 \left(\frac{1}{\alpha} \log \left(\frac{1}{\beta} \right) + \frac{1}{\alpha} \log \left(\frac{1}{\alpha} \right) \right)$, where κ_0 is some universal constant, we have that with probability at least $1 - \beta$,

$$\text{Err}(f_{\text{lin},\hat{\rho}}; \mathcal{D}^{c,\rho}) \leq \alpha.$$

Non-linear robust solution Next, we propose an algorithm to find a robust solution and show that this solution has a non-linearity of degree k . First, sample the m -sized dataset S_m and use the method described above to find $\hat{\rho}$. Then, create a modified dataset \hat{S} by first removing all points \mathbf{x} from S_m such that $|x[0] - \hat{\rho}| \geq \frac{\epsilon}{8}$ and then removing the first coordinate of the remaining points. Thus, each element in \hat{S} belongs to $\mathbb{R}^p \times \{0, 1\}$ dimensional dataset.

Note, that by construction, there is a consistent (i.e., an accurate) parity classifier on \hat{S} . Let the parity bit vector consistent with \hat{S} be $\hat{\mathbf{c}}$. This can be learned using Gaussian elimination. Consequently, construct the parity classifier $f_{\text{par},\hat{\mathbf{c}}} = \sum_{i=0}^{p-1} \hat{\mathbf{x}}[i] \cdot \hat{\mathbf{c}}[i] \pmod{2}$.

Finally, the algorithm returns the classifier $g_{\hat{\rho},\hat{\mathbf{c}}}$, which acts as follows:

$$g_{\hat{\rho},\hat{\mathbf{c}}}(\mathbf{x}) = \begin{cases} 1 & \mathbb{I}\{x[0] \geq \hat{\rho} + \epsilon + \frac{\epsilon}{8}\} \\ 0 & \mathbb{I}\{x[0] \leq \hat{\rho} - \epsilon - \frac{\epsilon}{8}\} \\ f_{\text{par},\hat{\mathbf{c}}}(\tilde{\mathbf{x}}) & \text{o.w.} \end{cases} \quad (8)$$

where $\tilde{\mathbf{x}} = \text{round}(\mathbf{x}[1], \dots, \mathbf{x}[p])$ is obtained by rounding off \mathbf{x} starting from the second index till the last. For example, if $\mathbf{x} = [0.99, 0.4, 0.9, 0.4, 0.8]$, $\epsilon = 0.2$, and $\mathbf{c} = [0, 0, 1, 1]$ then $\tilde{\mathbf{x}} = [0, 1, 0, 1]$ and $g_{0.5,\hat{\mathbf{c}}}(\tilde{\mathbf{x}}) = 1$. Finally, it is easy to verify that the classifier $g_{\hat{\rho},\hat{\mathbf{c}}}$ is accurate on all training points and as the number of total parity classifiers is less than 2^p (hence finite VC dimension), as long as $m \geq \kappa_1 \left(\frac{1}{\alpha} \log \left(\frac{1}{\beta} \right) + \frac{p}{\alpha} \log \left(\frac{1}{\alpha} \right) \right)$, where κ_1 is some universal constant, we have that with probability at least $1 - \beta$,

$$\text{Err}(g_{\hat{\rho},\hat{\mathbf{c}}}; \mathcal{D}^{c,\rho}) \leq \alpha.$$

Robustness of $g_{\hat{\rho},\hat{\mathbf{c}}}$ As $x[0]$ is distributed uniformly in the intervals $[\rho - \epsilon, \rho] \cup [\rho, \rho + \epsilon]$, we have that $|\rho - \hat{\rho}| \leq 4\epsilon \cdot \text{Err}(f_{\text{lin},\hat{\rho}}; \mathcal{D}^{c,\rho}) \leq 4\epsilon\alpha$. Therefore, when m is large enough ($m = \text{poly}(\frac{1}{\alpha})$) such that $\alpha \leq \frac{1}{32}$, we have that $|\hat{\rho} - \rho| \leq \frac{\epsilon}{8}$. Intuitively, this guarantees that $g_{\hat{\rho},\hat{\mathbf{c}}}$ uses the linear threshold function on $x[0]$ for classification in the interval $[\rho, \rho + \epsilon] \cup [\rho, \rho - \epsilon]$ and $f_{\text{par},\hat{\mathbf{c}}}$ in the $[\rho + 2\epsilon, \rho + 3\epsilon] \cup [\rho - 2\epsilon, \rho - 3\epsilon]$. A crucial property of $g_{\hat{\rho},\hat{\mathbf{c}}}$ is that for all $\mathbf{x} \in \text{Supp}(\mathcal{D}^{c,\rho})$, the classifier $g_{\hat{\rho},\hat{\mathbf{c}}}$ does not alter its prediction in an ℓ_∞ -ball of radius ϵ . We show this by studying four separate cases. First, we prove robustness along all coordinates except the first.

1. When $|x[0] - \hat{\rho}| \geq \epsilon + \frac{\epsilon}{8}$, as shown above, $g_{\hat{\rho},\hat{\mathbf{c}}}$ is invariant to all $x[i]$ for all $i > 0$ and is thus robust against all ℓ_∞ perturbations against those coordinates.

⁴<https://www.cs.ox.ac.uk/people/varun.kanade/teaching/CLT-MT2018/lectures/lecture03.pdf>

2. When $|\mathbf{x}[0] - \hat{\rho}| < \epsilon + \frac{\epsilon}{8}$, due to Equation (8), we have that $g_{\hat{\rho}, \hat{c}} = f_{\text{par}, \hat{c}}(\tilde{\mathbf{x}})$ where $\tilde{\mathbf{x}} = \text{round}(\mathbf{x}[1, \dots, p])$ is obtained by rounding off all indices of \mathbf{x} except the first. As the rounding operation on the boolean hypercube is robust to any ℓ_∞ perturbation of radius less than 0.5, we have that $g_{\hat{\rho}, \hat{c}}$ is robust to all ℓ_∞ perturbations of radius less than 0.5 on the support of the distribution $\mathcal{D}^{c, \rho}$.

Next, we prove the robustness along the first coordinate. Let $0 < \delta < \epsilon$ represent an adversarial perturbation. Without loss of generality, assume that $\mathbf{x}[0] > \hat{\rho}$ as similar arguments apply for the other case.

1. Consider the case $\mathbf{x}[0] \leq \hat{\rho} + \epsilon + \frac{\epsilon}{8}$. Then, $|\mathbf{x}[0] - \delta - \hat{\rho}| \leq |\epsilon + \frac{\epsilon}{8} - \delta| \leq \epsilon + \frac{\epsilon}{8}$ and hence, by construction, $g_{\hat{\rho}, \hat{c}}(\mathbf{x}) = g_{\hat{\rho}, \hat{c}}([\mathbf{x}[0] - \delta; \mathbf{x}[1, \dots, p]])$. On the other hand, for all δ , we have that $g_{\hat{\rho}, \hat{c}}([\mathbf{x}[0] + \delta; \mathbf{x}[1, \dots, p]]) = 1$ if $g_{\hat{\rho}, \hat{c}}(\mathbf{x}) = 1$.
2. For the case $\mathbf{x}[0] \geq \hat{\rho} + \epsilon + \frac{\epsilon}{8}$, the distribution is supported only on the interval $[\rho + 2\epsilon, \rho + 3\epsilon]$. When a positive δ is added to the first coordinate, the classifier's prediction does not change and it remains 1. For all $\delta \leq \frac{\epsilon}{2}$, when the perturbation is subtracted from the first coordinate, its first coordinate is still larger than $\hat{\rho} + \epsilon + \frac{\epsilon}{8}$ and hence, the prediction is still 1.

This completes the proof of robustness of $g_{\hat{\rho}, \hat{c}}$ along all dimensions to ℓ_∞ perturbations of radius less than ϵ . Combining this with its error bound, we have that $\text{Adv}_{\epsilon, \infty}(g_{\hat{\rho}, \hat{c}}; \mathcal{D}^{c, \rho}) \leq \alpha$.

To show that the parity function is non-linear, we use a classical result from Aspnes et al. [4]. Theorem 2.2 in Aspnes et al. [4] shows that approximating the parity function in k bits using a polynomial of degree ℓ incurs at least $\sum_{i=0}^{k_\ell} \binom{k}{i}$ where $k_\ell = \lfloor \frac{k-\ell-1}{2} \rfloor$ mistakes. Therefore, the lowest degree polynomial that can do the approximation accurately is at least k .

This completes our proof of showing that the robust classifier is of non-linear degree k while the accurate classifier is linear. Next, we prove that no linear classifier can be robust. We show this by contradiction.

No linear classifier can be robust Construct a set \mathcal{Z} of s (to be defined later) points in \mathbb{R}^{p+1} by sampling the first coordinate from the interval $[\rho, \rho + \epsilon]$ and the remaining p coordinates uniformly from the boolean hypercube. Then, augment the set by subtracting ϵ from the first coordinate while retaining the rest of the coordinates. Note that this set can be generated, along with its labels, by sampling enough points from the original distribution and discarding points that do not fall in this interval. Now construct adversarial examples of each point in the augmented set by either adding or subtracting ϵ from the negatively and the positively labelled examples respectively and augment the original set with these adversarial points. For a large enough s ,⁵ this augmented set of points can be decomposed into a multiset of points, where all points in any one set has the same value in the first coordinate but nearly half of their label is zero and the other half one.

Now, assume that there is a linear classifier that has a low error on the distribution $\mathcal{D}^{c, \rho}$. Therefore the classifier is also accurate on these sets of points as the classifier is robust, by assumption, and the union of these sets occupy a significant under the distribution $\mathcal{D}^{c, \rho}$. However, as the first coordinate of every point within a set is constant despite half the points having label one and the other half zero, the coefficient of the linear classifier can be set to zero without altering the behavior of the classifier. Then, effectively the linear classifier is representing a parity function on the rest of the p coordinates. However, we have just seen that this is not possible as a linear threshold function cannot represent a parity function on k bits where $k > 1$. This contradicts our initial assumption that there is a robust linear classifier for this problem.

This completes the proof. □

⁵There is a slight technicality as we might not obtain points that are exact reflections of each other around ρ but that can be overcome by discretising upto a certain precision

B Analysis of the separability of the intervened data

With the aim to illustrate how the interaction between \mathcal{D} and \mathcal{V} can influence the robustness of a classifier trained on $\tilde{\mathcal{D}}_\beta$ we now provide a toy theoretical example in which we discuss this interaction. Specifically, without loss of generality, consider the binary classification setting on the dataset $(\mathbf{x}, y) \sim \mathcal{D}$ where $y \in \{-1, +1\}$ and $\|\mathbf{x}\|_2 = 1$, for ease. Let's now consider the injected dataset $\tilde{\mathcal{D}}_\beta$ and further assume that $\mathbf{v}(+1) = \mathbf{u}$ and $\mathbf{v}(-1) = -\mathbf{u}$ with $\mathbf{u} \in \mathbb{R}^d$ and $\|\mathbf{u}\|_2 = 1$, such that $\tilde{\mathbf{x}} = \mathbf{x} + \beta y \mathbf{u}$. Moreover, let $\gamma \in [0, 1]$ denote the *interaction coefficient* between \mathcal{D} and \mathcal{V} , such that $-\gamma \leq \mathbf{x}^\top \mathbf{u} \leq \gamma$.

We are interested in characterizing the robustness of a classifier that only uses information in \mathcal{V} when classifying $\tilde{\mathcal{D}}_\beta$ depending on the strength of the interaction coefficient. In particular, as we are dealing with the binary setting, we will characterize the robustness of a linear classifier $h : \mathbb{R}^d \rightarrow \{-1, +1\}$ that discriminates the data based only on \mathcal{V} , i.e., $h(\tilde{\mathbf{x}}) = \text{sign}(\mathbf{u}^\top \tilde{\mathbf{x}})$. In our setting, we have

$$\begin{aligned} \mathbf{u}^\top \tilde{\mathbf{x}} &= \mathbf{u}^\top \mathbf{x} + \beta \mathbf{u}^\top \mathbf{u} = \mathbf{u}^\top \mathbf{x} + \beta \quad \text{if } y = +1 \\ \mathbf{u}^\top \tilde{\mathbf{x}} &= \mathbf{u}^\top \mathbf{x} - \beta \mathbf{u}^\top \mathbf{u} = \mathbf{u}^\top \mathbf{x} - \beta \quad \text{if } y = -1 \end{aligned}$$

Proposition 1 (Clean performance). *If $\beta > \gamma$, then h achieves perfect classification accuracy on $\tilde{\mathcal{D}}_\beta$.*

Proof. Observe that if $\gamma = 0$, i.e. the features from original dataset \mathcal{D} do not interact with the injected features \mathcal{V} , the dataset is perfectly linearly separable. However, if the data \mathbf{x} from \mathcal{D} interacts with the injected signal \mathbf{u} , i.e. non zero projection, then the dataset is still perfectly separable but for a sufficiently larger β , such that $\mathbf{u}^\top \mathbf{x} + \beta > 0$ when $y = +1$ and $\mathbf{u}^\top \mathbf{x} + \beta < 0$ when $y = -1$. Because $-\gamma \leq \mathbf{x}^\top \mathbf{u} \leq \gamma$ this is achieved for $\beta > \gamma$. \square

Proposition 2 (Robustness). *If $\beta > \gamma$, the linear classifier h is perfectly accurate and robust to adversarial perturbations in an ℓ_2 -ball of radius $\epsilon \leq \beta - \gamma$. Or, equivalently, for h to be ϵ -robust, the injected features must have a strength $\beta \geq \epsilon + \gamma$.*

Proof. Given $\tilde{\mathbf{x}}$, we seek to find the minimum distance to the decision boundary of such a classifier. A minimum distance problem can be cast as solving the following optimization problem:

$$\epsilon^*(\tilde{\mathbf{x}}) = \min_{\mathbf{r} \in \mathbb{R}^d} \|\mathbf{r} - \tilde{\mathbf{x}}\|_2^2 \quad \text{subject to } \mathbf{r}^\top \mathbf{u} = 0,$$

which can be solved in closed form

$$\epsilon^*(\tilde{\mathbf{x}}) = \frac{|\mathbf{u}^\top \tilde{\mathbf{x}}|}{\|\mathbf{u}\|} = |\mathbf{u}^\top \mathbf{x} + y\beta|.$$

The robustness radius of the classifier h will therefore be $\epsilon = \inf_{\tilde{\mathbf{x}} \in \text{supp}(\tilde{\mathcal{D}}_\beta)} \epsilon^*(\tilde{\mathbf{x}})$, which in our case can be bounded by

$$\epsilon = \inf_{(\tilde{\mathbf{x}}, y) \in \text{supp}(\tilde{\mathcal{D}}_\beta)} \epsilon^*(\tilde{\mathbf{x}}) \leq \min_{|\mathbf{u}^\top \mathbf{x}| \leq \gamma, y = \pm 1} |\mathbf{u}^\top \mathbf{x} + y\beta| = |\mp \gamma \pm \beta| = \beta - \gamma.$$

\square

Based on these propositions, we can clearly see that the interaction coefficient γ reduces the robustness of the additive features \mathcal{V} . In this regard, if $\epsilon \geq \beta - \gamma$, robust classification at a radius ϵ can only be achieved by also leveraging information within \mathcal{D} .

C Experimental details

In this section we provide the experimental details for all results presented in the paper. Adversarial training for all methods and datasets follows the fast training schedules with a cyclic learning rate introduced in [41]. We train for 30 epochs on CIFAR [17] and 15 epochs for SVHN [24] following

[2]. When we perform PGD-AT we use 10 steps and a step size $\alpha = 2/255$; FGSM uses a step size of $\alpha = \epsilon$. Regularization parameters for GradAlign [2] and N-FGSM [6] will vary and are stated when relevant in the paper. The architecture employed is a PreactResNet18 [11]. Robust accuracy is evaluated by attacking the trained models with PGD-50-10, i.e. PGD with 50 iterations and 10 restarts. In this case we also employ a step size $\alpha = 2/255$ as in [41]. All accuracies are averaged after training and evaluating with 3 random seeds.

The curvature computation is performed following the procedure described in Moosavi-Dezfooli et al. [23]. As they propose, we use finite differences to estimate the directional second derivative of the loss with respect to the input, *i.e.*,

$$w^\top \nabla_x^2 \mathcal{L}(f_\theta(x), y) \approx \frac{\nabla_x \mathcal{L}(f_\theta(x + tw), y) - \nabla_x \mathcal{L}(f_\theta(x - tw), y)}{2t},$$

with $t > 0$ and use the Lanczos algorithm to perform a partial eigendecomposition of the Hessian without the need to compute the full matrix. In particular, we pick $t = 0.1$.

All our experiments were performed using a cluster equipped with GPUs of various architectures. The estimated compute budget required to produce all results in this work is around 2,000 GPU hours (in terms of NVIDIA V100 GPUs).

D Inducing catastrophic overfitting with other settings

In Section 4 we have shown that CO can be induced with data interventions for CIFAR-10 and ℓ_∞ perturbations. Here we present similar results when using other datasets (i.e. CIFAR-100 and SVHN) and other types of perturbations (i.e. ℓ_2 attacks). Moreover, we also report results when the injected features $v(y)$ follow random directions (as opposed to low-frequency DCT components). Overall, we find similar findings to those reported the main text.

D.1 Other datasets

Similarly to Section 4 we intervene the SVHN and CIFAR-100 datasets to inject highly discriminative features $v(y)$. Since SVHN also has 10 classes, we use the exact same settings as in CIFAR-10 and we train and evaluate with $\epsilon = 4$ where training on the original data does not lead to CO (recall $\beta = 0$ corresponds to the unmodified dataset). On the other hand, for CIFAR-100 we select $v(y)$ to be the 100 DCT components with lowest frequency and we present results with $\epsilon = 5$. In both datasets we can observe similar trends as with CIFAR-10. For small values of β the injected features are not very discriminative due to their interaction with the dataset images and the model largely ignores them. As we increase β , there is a range in which they become more discriminative but not yet robust and we observe CO. Finally for large values of β the injected features become robust and the models can achieve very good performance focusing only on those.

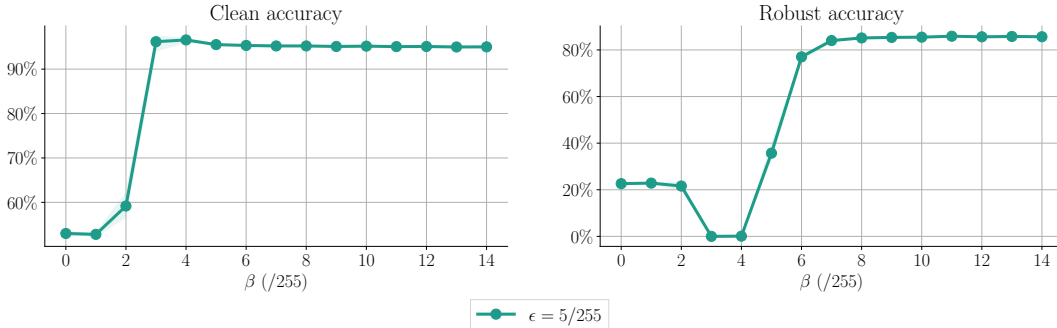


Figure 9: Clean and robust performance after FGSM-AT on intervened datasets $\tilde{\mathcal{D}}_\beta$ constructed from CIFAR-100. As FGSM-AT already suffers CO on CIFAR-100 at $\epsilon = 6/255$ we use $\epsilon = 5/255$ in this experiment where FGSM-AT does not suffer from CO as seen for $\beta = 0$. In this setting, we observe CO happening when β is slightly smaller than ϵ . Results are averaged over 3 seeds and shaded areas report minimum and maximum values.

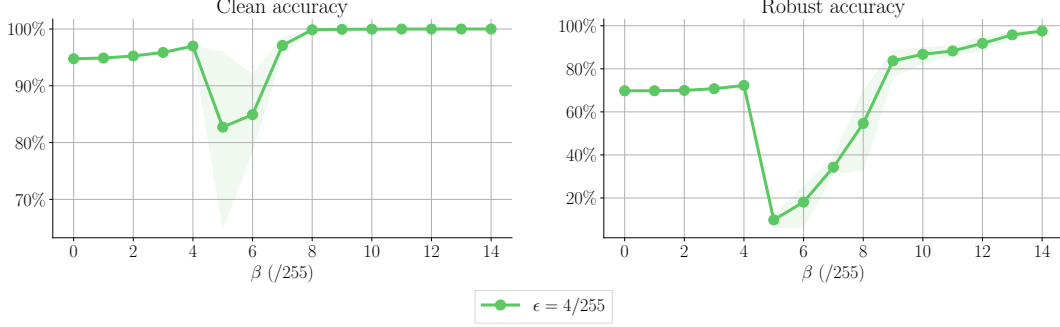


Figure 10: Clean and robust performance after FGSM-AT on intervened datasets $\tilde{\mathcal{D}}_\beta$ constructed from SVHN. As FGSM-AT already suffers CO on SVHN at $\epsilon = 6/255$ we use $\epsilon = 4/255$ in this experiment where FGSM-AT does not suffer from CO as seen for $\beta = 0$. In this setting, we observe CO happening when $\beta \approx \epsilon$. Results are averaged over 3 seeds and shaded areas report minimum and maximum values.

D.2 Other norms

Catastrophic overfitting has been mainly studied for ℓ_∞ perturbations and thus we presented experiments with ℓ_∞ attacks following related work. However, in this section we also present results where we induce CO with ℓ_2 perturbation which are also widely used in adversarial robustness. In Fig. 11 we show the clean (left) and robust (right) accuracy after FGM-AT⁶ on our intervened dataset from CIFAR-10 ($\tilde{\mathcal{D}}_\beta$). Similarly to our results with ℓ_∞ attacks, we also observe CO as the injected features become more discriminative (increased β). It is worth mentioning that the ℓ_2 norm we use ($\epsilon = 1.5$) is noticeably larger than typically used in the literature, however, it would roughly match the magnitude of an ℓ_∞ perturbation with $\epsilon = 7/255$. Interestingly, we did not observe CO for this range of β with $\epsilon = 1$.

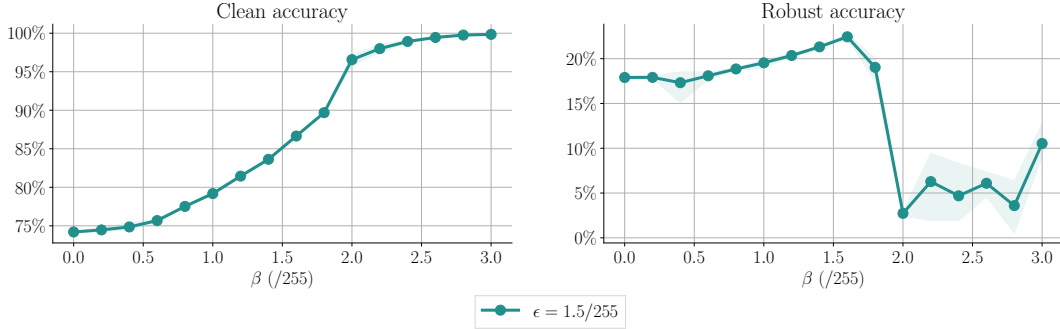


Figure 11: Clean and ℓ_2 robust performance after FGM-AT on intervened datasets $\tilde{\mathcal{D}}_\beta$ constructed from CIFAR-10. FGM-AT suffers CO on CIFAR-10 around $\epsilon = 2$, so we use $\epsilon = 1.5$ in this experiment where FGM-AT does not suffer from CO as seen for $\beta = 0$. In this setting, we observe CO happening when $\beta \approx \epsilon$. Results are averaged over 3 seeds and shaded areas report minimum and maximum values.

D.3 Other injected features

We selected the injected features for our intervened dataset from the low frequency components of the DCT to ensure an interaction with the features present on natural images [1]. However, this does not mean that other types of features could not induce CO. In order to understand how unique was our choice of features we also created another family of intervened datasets but this time using a set of 10 randomly generated vectors as features. As in the main text, we take the sign of each random

⁶FGM is the ℓ_2 version of FGSM where we do not take the sign of the gradient.

vector to ensure they take values in $\{-1, +1\}$ and assign one vector per class. In Fig. 12 we observe that using random vectors as injected features we can also induce CO. Note that since our results are averaged over 3 random seeds, each seed uses a different set of random vectors.

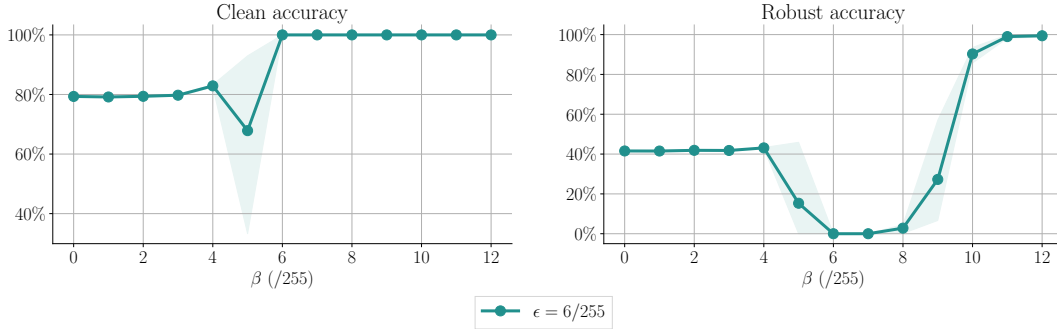


Figure 12: Clean and robust performance after FGSM-AT on intervened datasets $\tilde{\mathcal{D}}_\beta$ constructed from CIFAR-10 using random signals in \mathcal{V} . We perform this experiments at $\epsilon = 6/255$ where we saw intervening the dataset with the DCT basis vectors did induce CO. In the random \mathcal{V} setting, we observe the same behaviour, with CO happening when $\beta \approx \epsilon$. Results are averaged over 3 seeds and shaded areas report minimum and maximum values.

E Learned features at different β

In Section 4 we discussed how, based on the strength of the injected features β , our intervened datasets seem to have 3 distinct regimes: (i) When β is small we argued that the network would not use the injected features as these would not be very helpful. (ii) When β would have a very large value then the network would only look at these features since they would be easy-to-learn and provide enough margin to classify robustly. (iii) Finally, there was a middle range of β usually when $\beta \sim \epsilon$ where the injected features would be strongly discriminative but not enough to provide robustness on their own. This regime is where we observe CO.

In this section we present an extension of Fig. 4 where we take FGSM trained models on the intervened datasets ($\tilde{\mathcal{D}}_\beta$) and evaluate them on three test sets: (i) The injected test set ($\tilde{\mathcal{D}}_\beta$) with the same features as the training set. (ii) The original dataset (\mathcal{D}) where the images are unmodified. (iii) The shuffled dataset ($\tilde{\mathcal{D}}_{\pi(\beta)}$) where the injected features are permuted. That is, the set of injected features is the same but the class assignments are shuffled. Therefore, the injected features will provide conflicting information with the features present on the original image.

In Fig. 13 we show the performance on the aforementioned datasets for three different values of β . For $\beta = 2/255$ we are in regime (i) : we observe that the tree datasets have the same performance, i.e. the information of the injected features does not seem to alter the result. Therefore, we can conclude the network is mainly using the features from the original dataset \mathcal{D} . When $\beta = 20/255$ we are in regime (ii) : the clean and robust performance of the network is almost perfect on the injected test set $\tilde{\mathcal{D}}_\beta$ while it is close to 0% (note this is worse than random classifier) for the shuffled dataset. So when the injected and original features present conflicting information the network aligns with the injected features. Moreover, the performance on the original dataset is also very low. Therefore, the network is mainly using the injected features. Lastly, $\beta = 8/255$ corresponds to regime (iii) : as discussed in Section 5.1, in this regime the network initially learns to combine information from both the original and injected features. However, after CO, the network seems to focus only on the injected features and discards the information from the original features.

F Analysis of curvature in different settings

In Fig. 5 (left) we track the curvature of the loss surface while training on different intervened datasets with either PGD-AT or FGSM-AT. We observe that (i) Curvature rapidly increases both for PGD-AT and FGSM-AT during the initial epochs of training. (ii) In those runs that presented CO, the curvature explodes around the 10th epoch along with the training accuracy. (iii) When training with the dataset

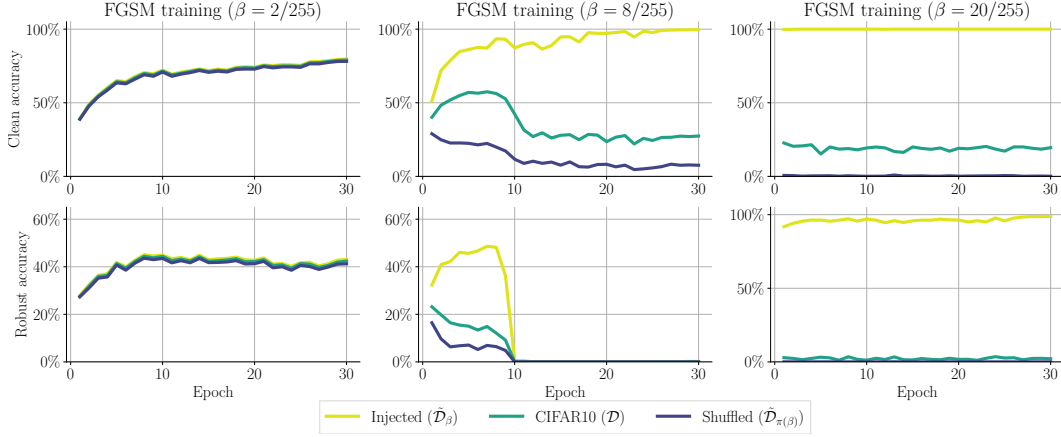


Figure 13: Clean (**top**) and robust (**bottom**) accuracy of FGSM-AT on $\tilde{\mathcal{D}}_\beta$ at different β values on 3 different test sets: (i) the original CIFAR-10 (\mathcal{D}), (ii) the dataset with injected features $\tilde{\mathcal{D}}_\beta$ and (iii) the dataset with shuffled injected features $\tilde{\mathcal{D}}_{\pi(\beta)}$. All training runs use $\epsilon = 6/255$. **Left:** $\beta = 2/255$ **Center:** $\beta = 8/255$ **Right:** $\beta = 20/255$.

with orthogonally injected features ($\tilde{\mathcal{D}}_\beta^\perp$) the curvature does not increase. This is aligned with our proposed mechanisms to induce CO whereby the network increases the curvature in order to combine different features to learn better representations. In this section we extend this analysis to the original CIFAR-10 dataset (as opposed to our intervened datasets) and to different values of feature strength β on the intervened dataset ($\tilde{\mathcal{D}}_\beta$). For details on how we estimate the curvature refer to Appendix C.

In Fig. 14 we show the curvature when training on the original CIFAR-10 dataset with $\epsilon = 8/255$ (where CO happens for FGSM-AT). Similarly to our observations on the intervened datasets, the curvature during FGSM-AT explodes along with the training accuracy while for PGD-AT the curvature increases at a very similar rate than FGSM-AT during the first epochs and later stabilizes. This indicates that our described mechanisms may as well apply to induce CO on natural image datasets.

On the other hand, Fig. 15 presents the curvature for different values of feature strength β on the intervened dataset ($\tilde{\mathcal{D}}_\beta$). We show three different values of β representative of the three regimes discussed in Appendix E. Recall that when β is small ($\beta = 2/255$) we observe that the model seems to focus only on CIFAR-10 features. Thus, we observe a curvature increase aligned with (CIFAR-10) feature combination. However, since for the chosen robustness radii $\epsilon = 6/255$ there is no CO, we observe that the curvature increase remains stable. When β is quite large ($\beta = 20/255$) then the model largely ignores CIFAR-10 information and focuses on the easy-to-learn injected features. Since these features are already robust, there is no need to combine them and the curvature does not need to increase. In the middle range when CO happens ($\beta = 8/255$) we observe again the initial curvature increase and then curvature explosion.

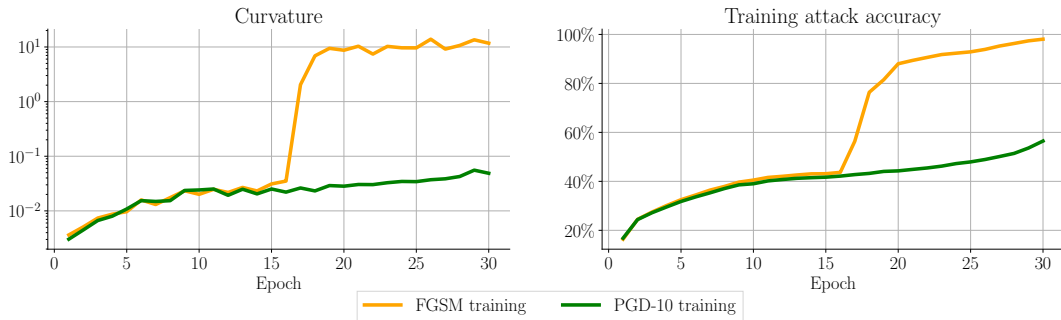


Figure 14: Evolution of curvature and training attack accuracy of FGSM-AT and PGD-AT trained on the original CIFAR-10 with $\epsilon = 8/255$. When CO happens the curvature explodes according to mechanism M3.

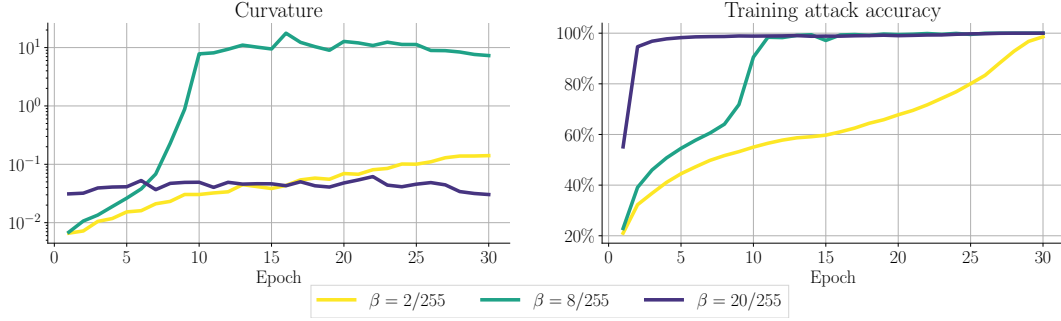


Figure 15: Evolution of curvature and training attack accuracy of FGSM-AT and PGD-AT trained on $\tilde{\mathcal{D}}_\beta$ at different β and for $\epsilon = 6/255$. Only when CO happens (for $\beta = 8/255$) the curvature explodes according to mechanism M3. For the other two interventions, because the network does not need to disentangle \mathcal{D} from \mathcal{V} , as it ignores either one of them, the curvature does not increase so much.

G Adversarial perturbations before and after CO

In order to further understand the change in behaviour after CO we presented visualizations of the FGSM perturbations before and after CO in Fig. 3. We observed that while prior to CO, the injected feature components $v(y)$ were clearly identifiable, after CO the perturbations do not seem to point in those directions although the network is strongly relying on them to classify. In Fig. 16 and Fig. 17 we show further visualizations of the perturbations obtained both with FGSM or PGD attacks on networks trained with either PGD-AT or FGSM-AT respectively.

We observe that when training with PGD-AT, i.e. the training does not suffer from CO, both PGD and FGSM attacks produce qualitatively similar results. In particular, all attacks seem to target the injected features with some noise due to the interaction with the features from CIFAR-10. For FGSM-AT, we observe that at the initial epochs (prior to CO) the perturbations are similar to those of PGD-AT, however, after CO perturbations change dramatically both for FGSM and PGD attacks. This aligns with the fact that the loss landscape of the network has dramatically changed, becoming strongly non-linear. This change yields single-step FGSM ineffective, however, the network remains vulnerable and multi-step attacks such as PGD are still able to find adversarial examples, which in this case do not point in the direction of discriminative features Jetley et al. [13], Ilyas et al. [12].

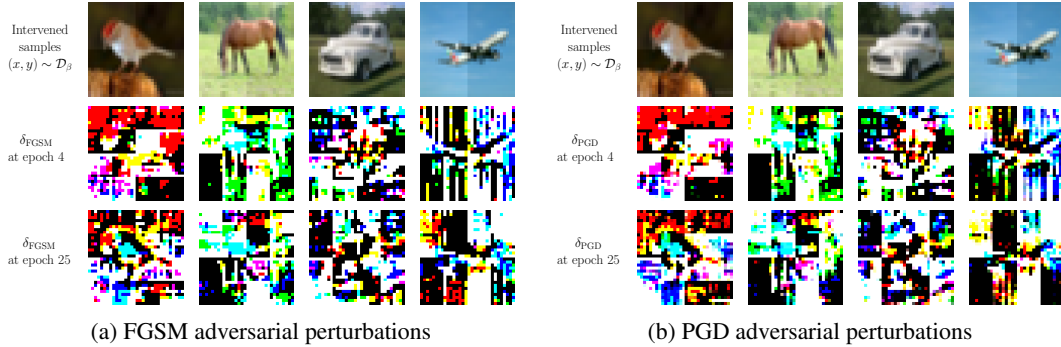


Figure 16: Different samples of the intervened dataset $\tilde{\mathcal{D}}_\beta$, and adversarial perturbations at epoch 4 and 22 of PGD-AT on $\tilde{\mathcal{D}}_\beta$ at $\epsilon = 6/255$ and $\beta = 8/255$ (where FGSM-AT suffers CO). The adversarial perturbations remain qualitatively similar throughout training and align significantly with \mathcal{V} .

H Further results with N-FGSM, GradAlign and PGD

In Section 6 we studied different SOTA methods that have been shown to prevent CO. Interestingly, we observed that in order to avoid CO on the intervened dataset a stronger level of regularization is needed. Thus, indicating that the intervention is strongly favouring the mechanisms that lead

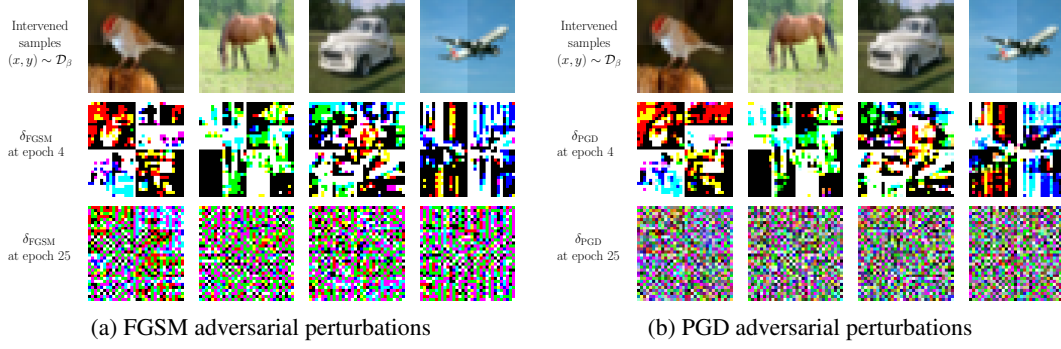


Figure 17: Different samples of the intervened dataset $\tilde{\mathcal{D}}_\beta$, and adversarial perturbations at epoch 4 (before CO) and 22 (after CO) of FGSM-AT on $\tilde{\mathcal{D}}_\beta$ at $\epsilon = 6/255$ and $\beta = 8/255$ (where FGSM-AT suffers CO). The adversarial perturbations change completely before and after CO. Prior to CO, they align significantly with \mathcal{V} , but after CO they point to meaningless directions.

to CO. For completeness, in Fig. 18 we also present results of the clean accuracy (again with the robust accuracy). As expected, for those runs in which we observe CO, clean accuracy quickly saturates. Note that for stronger levels of regularization the clean accuracy is lower. An ablation of the regularization strength might help improve results further, however the purpose of this analysis is not to improve the performance on the intervened data but rather to show it is indeed possible to prevent CO with the same methods that work for unmodified datasets.

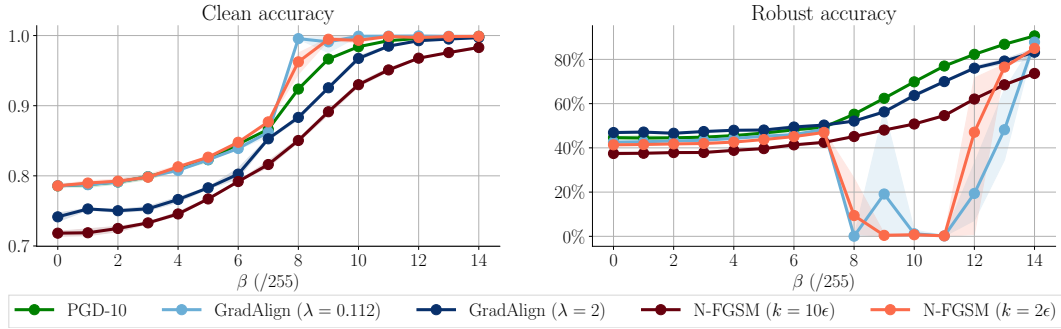


Figure 18: Clean (left) and robust (right) accuracy after AT with PGD-10, GradAlign and N-FGSM on $\tilde{\mathcal{D}}_\beta$ at $\epsilon = 6/255$. Results averaged over three random seeds and shaded areas report minimum and maximum values.

I Further details of low-pass experiment

We expand here over the results in Section 6 and provide further details on the experimental settings of Table 1. Specifically, we replicate the same experiment, *i.e.*, training a low-pass version of CIFAR-10 using FGSM-AT at different filtering bandwidths. As indicated in Section 6 we use the low-pass filter introduced in Ortiz-Jimenez et al. [26] which only retains the frequency components in the upper left quadrant of the DCT transform of an image. That is, a low-pass filter of bandwidth W would retain the $W \times W$ upper quadrant of DCT coefficients of all images, setting the rest of the coefficients to 0.

Figure 19 shows the robust accuracy obtained by FGSM-AT on CIFAR-10 versions that have been pre-filtered using such a low-pass filter. Interestingly, while training on the unfiltered images does induce CO on FGSM-AT, just removing a few high-frequency components is enough to prevent CO $\epsilon = 8/255$. However, as described before, it seems that at $\epsilon = 16/255$ no frequency transformation can avoid CO. Clearly, this transformation cannot be used as technique to prevent CO, but it highlights once again that the structure of the data plays a significant role in inducing CO.

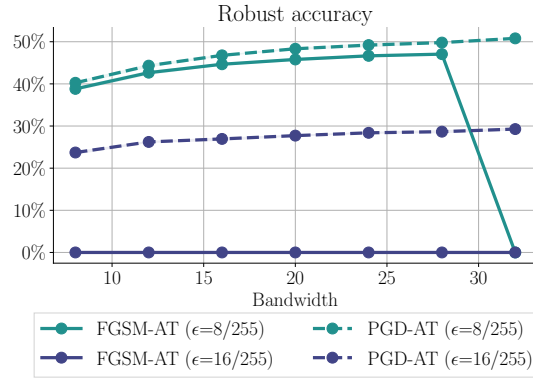


Figure 19: Robust accuracy of FGSM-AT and PGD-AT on different low-passed versions of CIFAR-10 using the DCT-based low pass filter introduced in Ortiz-Jimenez et al. [26]. Bandwidth = 32 corresponds to the original CIFAR-10, while smaller bandwidths remove more and more high-frequency components. At $\epsilon = 8/255$ just removing a few high-frequency components is enough to prevent CO, while at $\epsilon = 16/255$ no frequency transformation avoids CO.